SYNTHESIS OF TRIBLOCK TERPOLYMER POLY(STYRENE-*B*-VINYLBENZYL METHYLPYRROLIDINIUM CHLORIDE-*B*-OCTYLSTYRENE) USING REVERSIBLE ADDITION-FRAGMENTATION CHAIN-TRANSFER POLYMERIZATION

A Thesis

by

MAHESH AGRAWAL

Submitted to the Office of Graduate and Professional Studies of
Texas A&M University
in partial fulfillment of the requirements for the degree of

MASTER OF SCIENCE

Chair of Committee,	Yossef A. Elabd
Committee Members,	Jodie Lutkenhaus
	Lei Fang
	Micah Green
Head of Department,	Arul Jayaraman

May 2020

Major Subject: Chemical Engineering

ABSTRACT

Polymerized ionic liquid (PIL) block copolymers can be used as solid-state membranes in alkaline fuel cells (AFCs) to extend AFC lifetime performance. Combining the multiple block chemistries synergizes the individual properties of each chemistry into one polymer membrane, forming a high-ion-conducting, chemically stable, mechanically-strong, water insoluble, free-standing film. Moreover, PIL block copolymers can exhibit an array of nanostructured morphologies, which can affect the ion conductivity of the polymer (a key property that is proportional to AFC power output).

Previously, only PIL diblock copolymers with limited morphologies and properties have been synthesized for the AFC. In this work, a PIL triblock terpolymer was synthesized providing more chemistries, more morphologies, and a wider property window. First, a diblock copolymer poly(styrene-*b*-vinylbenzyl chloride) [poly(S-*b*-VBC)] was synthesized *via* reversible addition-fragmentation chain-transfer (RAFT) polymerization and the effect of chain transfer agent, and monomer and initiator concentrations were investigated at a small scale (*ca.* 1 g). Once the optimum conditions were determined at a small scale, poly(S-*b*-VBC) synthesis was successfully scaled-up to a larger scale (*ca.* 50 g) with narrow dispersity and well-defined molecular weight. Poly(S-*b*-VBC) was further chain extended using 4-octylstyrene and subsequently functionalized with *N*-methylpyrrolidine to obtain a PIL triblock terpolymer, poly(styrene-*b*-vinylbenzyl methylpyrrolidinium chloride-*b*-octylstyrene) [poly(S-*b*-VBMPyr-Cl-*b*-OS)]. Preliminary studies were performed on this PIL triblock terpolymer to study the thermal

properties (glass transition temperature and degradation temperature) and morphology. Further studies on this PIL triblock terpolymer at various compositions will allow for the exploration of a broader range of membrane properties and therefore the ability to tailor AFC performance.

ACKNOWLEDGEMENTS

I would like to begin by thanking my advisor, Professor Yossef A. Elabd, for his guidance and support through each stage of my research. Thank you for being a constant source of inspiration and giving me a chance to grow professionally and personally! I am also highly grateful to my dissertation committee for their persistent help on improving my research. I would like to express my gratitude towards past and present members of Elabd research group, especially, Patrick, Rui and Monica for their mentorship and unending support on my research work. My sincere acknowledgement goes to all my friends who helped me complete this journey! Finally, I would like to express my heartfelt gratitude towards my family for their encouragement and unwavering support. Thank you!

CONTRIBUTORS AND FUNDING SOURCES

Contributors

This work was supervised by a thesis committee consisting of Professor Yossef A. Elabd, Professor Micah Green and Professor Jodie Lutkenhaus of the Department of Chemical Engineering and Professor Lei Fang of the Department of Chemistry.

The small angle X-ray scattering characterization for Chapter 3 was performed at Soft Matter Facility (SoMF), Texas A&M University.

Funding Sources

This work is supported in part by the National Science Foundation under Grant No. CBET-1703645.

TABLE OF CONTENTS

Page

Page

LIST OF FIGURES

Page

LIST OF TABLES

Page

1. INTRODUCTION

1.1. Need for Clean Energy

A recent report by the US Environmental Protection Agency shows that transportation accounts for one-third of the total carbon dioxide emitted from different sectors, such as industry, electricity, non-fossil fuel combustion, residential and commercial sectors.[1] This is because most of the 1.1 billion vehicles currently in use worldwide operate on internal combustion engines (ICEs). Replacing ICE vehicles with zero-emission vehicles such as hydrogen-fueled proton exchange membrane (PEM) fuel cells (*e.g.,* Toyota Mirai) or by rechargeable lithium ion batteries (*e.g.,* Tesla Model 3) would be an ideal solution for reducing carbon dioxide emissions. Compared to battery operated vehicles, fuel cell vehicles have advantages including lower vehicle weight (for a driving range over 250 miles), faster re-fueling, and six times higher specific energy density.[2, 3]

Presently, PEM fuel cell technology is expensive due to the use of noble metal catalysts (*e.g.,* platinum) required to facilitate facile oxygen reduction at the cathode. Meanwhile, alkaline fuel cells (AFCs) can utilize non-noble metal catalysts (*e.g.,* nickel) owing to inherent higher oxygen reduction kinetics in alkaline environments.[4] The use of non-noble metal catalysts in AFCs can significantly reduce the cost of fuel cell production and increase the viability of large scale commercialization.

1.2. Alkaline Fuel Cells

Alkaline fuel cells (AFCs) are electrochemical devices, which convert chemical energy into electrical energy. AFCs can produce high power density at low operating temperatures (< 200 °C). As shown in Figure 1.1, AFCs consist of an anode, a cathode and an electrolyte separating the two electrodes. The electrodes are connected by an external circuit. Typically, AFCs use a potassium hydroxide solution as the electrolyte for hydroxide ion transport.

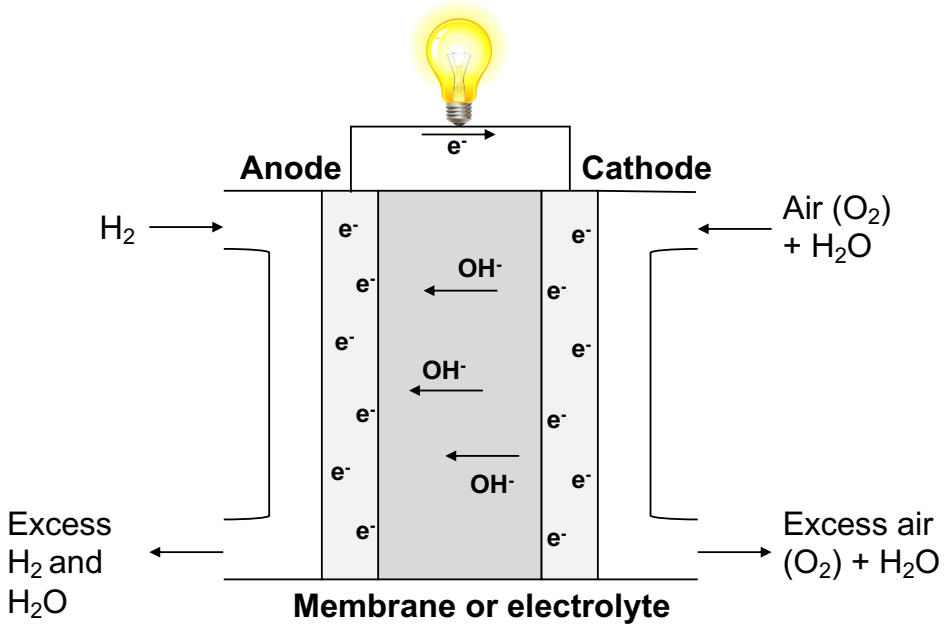

Figure 1.1 Alkaline fuel cell.

Anode: $2H_2 + 4OH^- \rightarrow 4H_2O + 4e^-$ **(1.1)**

Cathode: $O_2 + 2H_2O + 4e^- \rightarrow 4OH^-$ **(1.2)**

Overall: $2H_2 + O_2 \rightarrow 2H_2O$ **(1.3)**

In AFC operation, hydrogen gas is oxidized with hydroxide ions at the anode to generate electrons and water (Reaction 1.1). The electrons travel through the external circuit to the cathode, where the electrons are reduced by oxygen and water (Reaction 1.2), generating hydroxide ions which diffuse back to the anode through the electrolyte. This process generates electricity as the product, and heat and water as byproducts (Reaction 1.3).

AFCs were employed in the NASA Apollo space missions as the primary source of electrical power for the spacecraft. During the Apollo 11 mission, three sets of fuel cell power houses, each containing 17 separate fuel cells in series, were used to generate the required electricity. The water generated during the fuel cell operation was used by astronauts as drinking water.

However, the AFC's biggest challenge is electrolyte management. The liquid electrolyte (KOH) can readily react with carbon dioxide impurities present in gases and form potassium carbonate (K_2CO_3) precipitates. The precipitates poison the fuel cell, reducing ion conductivity, degrading catalyst performance, and severely declining AFC performance and lifetime.[5]

An appropriate remedy for electrolyte poisoning would be the use of solid-state ion-conducting membranes as alternatives to liquid electrolytes. The solid-state nature of

the membrane will address the concerns of electrolyte poisoning by lowering membrane sensitivity to carbon dioxide impurities. The carbon dioxide can still react with mobile hydroxide ions, but cannot form precipitates due to the absence of mobile cations (K^+).[5]

Furthermore, an ideal membrane for the AFC would be one that can deliver high hydroxide ion conductivity and high alkaline chemical stability, while also possessing high mechanical durability and flexibility. Polymerized ionic liquids (PILs) are a potential material that provide all of these desired properties in one solid-state material.

1.3. Polymerized Ionic Liquids

Previous studies exploring the possibility of using membranes in AFCs have shown that PILs are easy to synthesize and can be used as solid-state membranes.[6-18] Recent studies have explored optimal backbone-cation pairs, which can deliver high alkaline chemical stability and high ion conductivity for AFCs.[15-18]

The trimethylammonium (TMA) cation has been the most frequently explored cation for AFCs due to its ease of functionalization, high conductivity and thermal stability.[8-14] Hibbs *et al.*[15] compared the chloride ion conductivity and alkaline stability of various cations attached to polyphenylene backbones; specifically, the cations benzylic TMA, benzylic pentamethylguanidinum, and benzylic *N*-methylimidazolium. The polymer functionalized with BTMA achieved the highest chloride ion conductivity of 18 mS cm^{-1} in liquid water and the least significant losses in ionic conductivity (33% loss after 2 weeks in 4 M KOH at 90 °C).

Recently, Meek *et al.*[16] compared the alkaline chemical stability (80 °C, 0.5 M KOH/D_2O, 1 week) of methacrylate-based PILs consisting of various covalently attached cations; specifically, trimethylammonium, butylimidazolium, butylpyrrolidinium and trimethylphosphonium. Results showed enhanced chemical stability of pyrrolidinium-based (10.3% polymer degradation) and imidazolium-based (33.5% polymer degradation) PILs relative to quaternary ammonium-based (94.8% polymer degradation) and phosphonium-based (polymer precipitated) PILs.

In a subsequent study, Meek *et al.*[17] compared the bromide ion conductivity and alkaline chemical stability (60 °C, 0.5 M KOH/D_2O, 1 week) of ethyl methacrylate, undecyl methacrylate, undecyl acrylate, and styrene-based PILs consisting of various covalently attached cations; specifically, butylimidazolium, trimethylammonium, and butylpyrrolidinium. The butylpyrrolidinium styrene-based PIL showed the highest alkaline chemical stability (0% polymer degradation in 1 week after exposure to 0.5 M KOH/D_2O at 60 °C), meanwhile, the benchmark styrene/BTMA pairing degraded 13.2% under the same conditions. Furthermore, the butylpyrrolidinium styrene-based PIL was able to achieve a high bromide ion conductivity (14.5 mS cm^{-1} at 60 °C and 90% RH) while the styrene/BTMA pairing showed lower conductivity (2.7 mS cm^{-1} under the same conditions).

More recently, Sun *et al.*[18] compared the bromide ion conductivity and alkaline chemical stability (80 °C, 1 M KOH/D_2O, 4 weeks) of styrene-based PIL containing saturated *N*-heterocyclic cations with various ring sizes; specifically, methylpyrrolidinium,

methylpiperidinium, methylazepanium, methylazocanium, and methylazonanium). High alkaline chemical stability was reported for methylpyrrolidinium-, methylpiperidinium-, and methylazepanium-based PILs (0% polymer degradation), which was attributed to the basicity and stability of cyclic cation. Furthermore, high bromide ion conductivity (19.2 mS cm^{-1}) was observed for the methylpyrrolidinium-based PIL at 80 °C and 90% RH.

These studies show the potential for use of styrene based PILs with a pyrrolidinium cation as solid-state membranes. However, these PIL homopolymers possess high water solubility and are not independently suitable for application as membranes in AFCs. One solution is employing PIL block copolymers, where combining a PIL homopolymers with a hydrophobic, mechanically-strong block can provide the desirable properties for solid-state membranes in AFCs: water insolubility, high alkaline stability, high ionic conductivity, and high mechanical strength.

1.4. PIL Block Copolymers

A block copolymer is a polymer comprised of a series of two or more polymer blocks in sequence, where each block possesses a unique chemistry with different physiochemical properties from the adjacent block(s). A class of block copolymers, PIL block copolymers, have one or more non-ionic polymer blocks attached to an ionic block, where the ionic block possesses ionic liquid chemistry. A representative PIL block copolymer is shown in

Figure 1.2, where polystyrene is the non-ionic block and poly(vinylbenzyl methylpyrrolidinium chloride) is the ion-conducting PIL block.

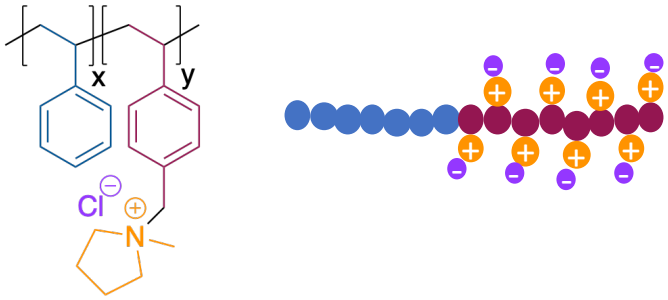

Figure 1.2 PIL block copolymer poly(styrene-*b*-vinylbenzyl methylpyrrolidinium chloride): (left) chemical structure, (right) illustration.

1.4.1. PIL Block Copolymer Synthesis

Block copolymers with well-defined molecular weight and narrow molecular weight distribution (*i.e.*, dispersity) can be synthesized using controlled living free radical polymerization reactions. Recently, PIL block copolymers have been synthesized using polymerization techniques such as nitroxide-mediated polymerization[19-24], atom transfer radical polymerization (ATRP)[25-28], anionic polymerization[29, 30], and reversible addition-fragmentation chain-transfer (RAFT) polymerization.[31-33] In this study, RAFT polymerization is employed as it can generate large quantities of block copolymers using a reflux condenser set-up (discussed further in Chapter 2).[31]

RAFT polymerization utilizes a chain transfer agent (CTA) to produce polymers with well-defined molecular weights.[34-38] One of the key considerations in RAFT polymerization reactions is the selection of the CTA. An appropriate CTA must be selected based on compatibility with the monomers to ensure successful polymerization reactions (discussed further in Chapter 2).[39-41]

Meek *et al*.[42] discussed two pathways to synthesize PIL block copolymer using RAFT polymerization: (1) sequential addition of non-ionic monomers and post-polymerization functionalization of one of the monomers, (2) direct sequential polymerization of non-ionic monomer with an ionic liquid monomer. It was also pointed out that the first strategy allows for facile molecular weight and dispersity analysis using size exclusion chromatography (SEC), meanwhile, in the latter strategy, addition of salt is required to screen the electrostatic repulsion and minimize charge aggregation when using SEC.[43]

1.4.2. PIL Diblock Copolymers

PIL diblock copolymers are comprised of a hydrophobic mechanical strengthening block and ion-conducting PIL block. On the submicron scale, these blocks usually form domains in the solid-state, and based on the immiscibility of the blocks, the domains can exhibit phase separation and arrange themselves into various nanostructures (*i.e.*, morphologies).[44]

Ye *et al.*[32] revealed that PIL diblock copolymers can exhibit microphase separation and deliver an order of magnitude higher conductivity than their analogous PIL

homopolymers, even though the homopolymers possess higher ion exchange capacities (IECs). This is due to presence of well-defined ion conducting pathways in PIL block copolymers, which are absent in both PIL random copolymers and PIL homopolymers. Previous studies in diblock copolymer systems have discovered the presence of four diblock morphologies: lamellar, cylindrical, gyroid and spherical.[45, 46] The various AB diblock morphologies are based on the interaction parameter (represented by χ_{AB}), the overall degree of polymerization (N) and the volume fraction of the two blocks represented by f_A and f_B (where, $f_B = 1 - f_A$).[47]

Furthermore, Choi *et al.*[48] have shown that morphology plays a significant role in determining the ion conductivity in PIL diblock copolymers. Their study analyzed solution cast films of the same polymer [poly(styrene-*b*-1-((2-acryloyloxy)ethyl)-3-butylimidazolium bis-(trifluoromethanesulfonyl)imide)] using two different solvents, where one of the solvents (tetrahydrofuran) preferred the non-ionic polystyrene block and other solvent (acetonitrile) preferred the ionic PIL block. This resulted in two polymer films with different morphologies (lamellar and network morphologies) and it was observed that the polymer film with the network morphology exhibited higher conductivity than the polymer film with the lamellar morphology. The reason for higher conductivity was attributed to the three-dimensional continuity of the network morphology. However, the network morphology can only be achieved in a small composition window of diblock copolymers. This issue can be addressed by the addition

of one more block to the diblock copolymer (resulting in triblock terpolymers), *i.e.*, more network morphologies and a larger compositional window to achieve these morphologies.

1.4.3. PIL Triblock Terpolymers

Triblock terpolymers can be synthesized by chain extension of diblock copolymers with another monomer (different from either of the monomers used in the synthesis of two blocks in the diblock copolymer). The addition of a third block to a diblock copolymer (to form an ABC triblock terpolymer) triples the number of χ interaction parameters (χ_{AB}, χ_{BC}, χ_{AC}), doubles the number of independent composition variables (f_A, f_B, $f_C = 1 - f_A - f_B$,) and triples the possible number of block sequences (ABC, ACB, BAC), resulting in multiple additional morphologies.[47]

Previous studies in the triblock terpolymer systems, *e.g.*, poly(isoprene-*b*-styrene-*b*-dimethylsiloxane),[49] poly(isoprene-*b*-styrene-*b*-ethylene oxide),[47, 50] and poly(styrene-*b*-2-vinylpyridine-*b*-tert-butyl methacrylate),[51] have shown the presence of multiple additional morphologies, many of the morphologies classified as three-dimensionally continuous (an ideal morphology for high ion conductivity).[50] Furthermore, the addition of a third block allows for the inclusion of additional physiochemical properties to the polymer (*e.g.*, flexibility), making the polymer film more robust for the AFC.

1.5. Summary

In this work, a PIL triblock terpolymer, poly(styrene-*b*-vinylbenzyl methylpyrrolidinium chloride-*b*-octylstyrene) (see Figure 1.3) was synthesized using RAFT polymerization. Hypothetically, this PIL triblock terpolymer can provide high alkaline chemical stability and high ion conductivity due to the presence of a PIL block, high mechanical strength due to presence of the polystyrene block (glass transition temperature (T_g) above operating temperature of AFC), and flexibility due to the presence of the polyoctylstyrene block (T_g below room temperature).

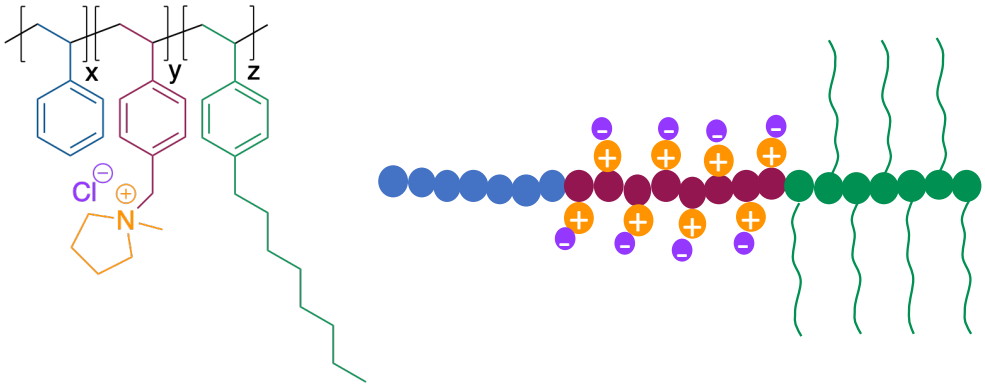

Figure 1.3 PIL triblock terpolymer poly(styrene-*b*-vinylbenzyl methylpyrrolidinium chloride-*b*-octylstyrene): (left) chemical structure, (right) illustration.

Chapter 2 focuses on developing the methodology for larger scale (50 g scale) synthesis of the diblock copolymer poly(styrene-*b*-vinylbenzyl chloride). Scaling up the polymer

synthesis is a cost-effective process of generating a larger quantity of polymer for characterization and future use (such as for chain extension or functionalization).

Chapter 3 is a study of chain extension of the diblock copolymer poly(styrene-*b*-vinylbenzyl chloride) using 4-octylstyrene monomer, resulting in the triblock terpolymer poly(styrene-*b*-vinylbenzyl chloride-*b*-octylstyrene). This triblock terpolymer was subsequently functionalized using pyrrolidinium based cation to obtain poly(styrene-*b*-vinylbenzyl methylpyrrolidinium chloride-*b*-octylstyrene). The functionalized triblock terpolymer can provide additional physiochemical properties and open the possibility of exploring numerous morphologies and their effect on polymer properties.

2. SCALING UP SYNTHESIS OF DIBLOCK COPOLYMER POLY(STYRENE-*B*-VINYLBENZYL CHLORIDE)

2.1. Introduction

This study focuses on developing a methodology to scale-up the synthesis of multiblock polymers synthesized using RAFT polymerization, *i.e.*, increasing production by orders of magnitude from typical 1 g scale quantities produced in academic laboratories. Scaling up polymerization results in more sample for characterization, a more cost-effective overall process, and higher feasibility for future commercialization.

One challenge with scaling up polymerization reactions is ensuring ideal mixing of the reacting mixture inside the reactor, thereby maintaining a homogenous mixture and uniform temperature throughout the solution. Ideal mixing could be achieved by employing reflux condensers, which creates convection currents in the reacting mixture and maintains uniform temperature. Hence, a reflux condenser was used for polymerizations in this study to increase the amount of polymer produced.

In this study, a reaction scheme was developed to synthesize diblock copolymer poly(styrene-*b*-vinylbenzyl chloride) at a larger scale (up to 50 g of diblock copolymer in one reaction) using RAFT polymerization. The polystyrene block provides the necessary hydrophobicity to the polymer and poly(vinylbenzyl chloride) block can easily be modified post-polymerization to form the ion-conducting block.[52-54]

In RAFT polymerization, the chemistry of the chain transfer agent (CTA) determines its compatibility with the monomer.[39-41] Hence, three different CTAs and their effect on RAFT polymerization of styrene and its further chain extension with vinylbenzyl chloride were investigated in this study.

2.2. Experimental Method

2.2.1. Materials

4-Cyano-4-[(dodecylsulfanylthiocarbonyl)sulfanyl]pentanoic acid (chain transfer agent, CTA1) was used as received from Fisher Scientific. 4-Cyano-4-(phenylcarbonothioylthio) pentanoic acid (CTA 2) was used as received from Sigma Aldrich. 2-cyanobutanyl-2-yl 3,5-dimethyl-1H-pyrazole-1-carbodithioate (CTA 3) was used as received from Boron Molecular. Chemical structures of all three CTAs used in this study are shown in Figure 2.1. Toluene (anhydrous, 99.8%), methanol (ACS Reagent, ≥99.8%), tetrahydrofuran (THF, ≥99.9%), tetrahydrofuran (HPLC THF, HPLC grade, ≥99.9%), chloroform-d ($CDCl_3$, 100%, 99.96 atom % D) were used as received from Sigma Aldrich. 4-vinylbenzyl chloride (90%, contains 500 ppm 4-tert-butylcatechol as stabilizer) and styrene (ReagentPlus, contains 4-tert-butylcatechol as stabilizer, ≥99%) were purchased from Sigma Aldrich and purified by passing through aluminum oxide before use. Azobis(isobutyronitrile) (AIBN, 98%, Sigma-Aldrich) was purified by recrystallization twice from methanol.

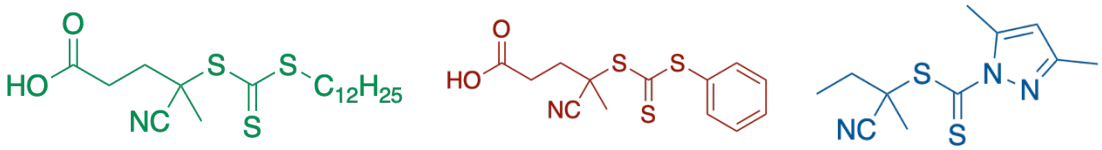

CTA 1 **CTA 2** **CTA 3**

Figure 2.1 Chain Transfer Agents (CTAs) used in this study.

2.2.2. Synthesis of PS-CTA at a 5 g Scale

The preparation of polystyrene chain transfer agent (PS-CTA) at a 5 g scale is shown in Scheme 2.1 (1). In a typical synthesis procedure, 10.01 g of styrene monomer, 243.4 mg of CTA3 and 10.05 g of toluene were mixed in a single neck 100 mL Schlenk flask. The flask was subjected to four freeze-pump-thaw degassing cycles followed by sealing the reactor and performing the reaction under static nitrogen at 100 ºC for 20 h. The resulting polymer was twice precipitated in methanol and dried under vacuum in an oven at room temperature for 24 h. Yield: 4.72 g of solid particles (98.34%). ^{1}H NMR (500 MHz, $CDCl_3$, 23 °C) δ (ppm): 7.28-6.28 (m, 5H, C_6H_5), 2.14-1.16 (m, 3H, CH_2-CH, CH_2-C*H*) (^{1}H NMR, Figure 2.3(c)); SEC (THF, 40 °C): M_n = 5.2 kg mol^{-1}, M_w/M_n = 1.17 (against PS standards) (Figure 2.2).

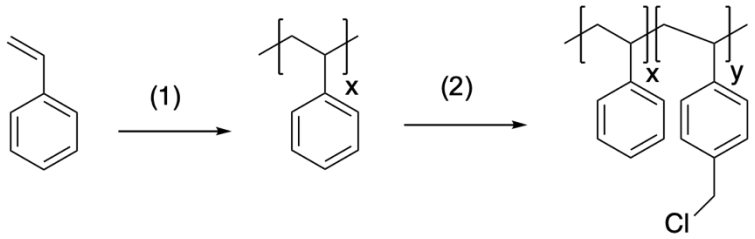

(1) CTA, Toluene, 20 h, 100 ºC; (2) VBC, AIBN, THF, 5h, 60 ºC

Scheme 2.1 Polymerization of (1) polystyrene and (2) poly(styrene-*b*-vinylbenzyl chloride).

2.2.3. Synthesis of PS-CTA at a 125 g Scale

The preparation of polystyrene chain transfer agent (PS-CTA) at a 125 g scale is shown in Scheme 2.1 (1). In a typical synthesis procedure, 250.63 g of styrene monomer, 6.0855 g of CTA3 and 250.06 g of toluene were mixed in a 1 L three-neck round-bottom-flask. The central neck of the flask was connected to a reflux condenser, which was connected to a nitrogen source and a bubbler. The other two necks of the flask were sealed by rubber septa. After sealing, the reactor was degassed by bubbling nitrogen through the reacting mixture for 1 hour. After degassing, the reaction was performed under reflux for 20 h. The resulting polymer was twice precipitated in methanol and dried under vacuum in an oven at room temperature for 24 h. Yield: 120.48 g of solid particles (98.10%). ^{1}H NMR (500 MHz, $CDCl_3$, 23 °C) δ (ppm): 7.28-6.28 (m, 5H, C_6H_5), 2.14-1.16 (m, 3H, CH_2-C*H*, CH_2-CH) (Figure 2.11 (a)); SEC (THF, 40 °C): M_n = 5.3 kg mol^{-1}, M_w/M_n = 1.18 (against PS standards) (Figure 2.9).

2.2.4. Synthesis of Poly(S-*b*-VBC) at a 1 g Scale

Diblock copolymer poly(styrene-*b*-vinylbenzyl chloride) [poly(S-*b*-VBC)] was synthesized by chain extension of PS-CTA. In a typical 1 g scale synthesis procedure, 1.011 g of PS-CTA3, 2.585 g of purified (by passing through aluminum oxide column) VBC monomer, 2.594 g of THF and 0.0019 g of AIBN were mixed in a 10 mL Schlenk flask. The flask was sealed and subjected to four freeze-pump-thaw operations. The sealed flask was then immersed in an oil bath at 60 ºC and the polymerization reaction was performed for 5 h. The resulting polymer was twice precipitated in methanol and dried under vacuum in an oven at room temperature for 24 h. Yield: 1.131 g of solid particles (99.1 %). SEC (THF, 40 °C): M_n = 7.2 kg mol^{-1}, M_w/M_n = 1.20 (against PS standards) (Figure 2.7).

2.2.5. Synthesis of Poly (S-*b*-VBC) at a 50 g Scale

The diblock copolymer poly(styrene-*b*-vinylbenzyl chloride) [poly(S-*b*-VBC)] was synthesized by chain extension of PS-CTA. In a typical 50 g scale reaction, 45.79 g of PS-CTA, 130.73 g of purified (by passing through aluminum oxide column) 4-vinylbenzyl chloride, 0.1410 g of AIBN and 130.70 g of THF were mixed together in a 500 mL three-neck round-bottom-flask. The central neck of the flask was connected to a reflux condenser, which was connected to a nitrogen source and a bubbler. The other two necks of the flask were sealed by rubber septa. After sealing, the reactor was degassed by

bubbling nitrogen through the reacting mixture for 1 h. After degassing, the reaction was performed under reflux for 5 h. The resulting polymer was thrice precipitated in methanol after dissolving in THF and dried under vacuum in an oven at room temperature for 48 h. Yield: 52.35 g of solid particles (99.4 %). ^{1}H NMR (500 MHz, $CDCl_3$, 23 °C) δ (ppm): 7.28-6.18 (m, 9H, C_6H_5, C_6H_4-CH_2), 4.67-4.29 (s, 2H, C_6H_4-CH_2), 2.14-1.16 (m, 3H, CH_2-CH, CH_2-C*H*) (Figure 2.11 (b)); SEC (THF, 40 °C): M_n = 7.6 kg mol^{-1}, M_w/M_n = 1.29 (against PS standards) (Figure 2.10).

2.3. Characterization

Molecular weights and molecular weight distributions of PS-CTA and poly(S-*b*-VBC) were determined by size exclusion chromatography (SEC) using Waters Gel Permeation Chromatography (GPC) system equipped with a THF Styragel column (Styragel@HR 5E, effective separation of molecular weight range: 2-4000 kg mol^{-1}) and a 2414 refractive index (RI) detector. All measurements were performed at 40 °C. HPLC THF was used as the mobile phase at a flow rate of 1.0 mL/min. PS standards (Shodex, Japan) with molecular weights ranging from 2.97 to 983 kg mol^{-1} were used for calibration.

Chemical structures and number-average molecular weights of PS-CTA and poly(S-*b*-VBC) were characterized by ^{1}H NMR spectroscopy using a Varian 500 MHz spectrometer at 23 °C with $CDCl_3$ as the solvent. All chemical peaks were referenced to chloroform peak ($CHCl_3$) at 7.27 ppm.

Glass transition temperature (T_g) was determined by differential scanning calorimetry (DSC; TA Instruments, Q200) over a temperature range of –140 ºC to 200 ºC at a heating/cooling rate of 10 ºC/min under a nitrogen environment (50 mL/min) using a heat/cool/heat method. T_g was determined using the midpoint method from the second thermogram heating cycle.

Thermal degradation temperature (T_d) was determined using thermogravimetry analysis (TGA; TA Instruments, Q50) over a temperature range of 25 °C to 900 °C at a heating rate of 10 ºC/min under a nitrogen environment (60 mL/min). The degradation temperature was determined at 5% weight loss.

2.4. Results and Discussions

Figure 2.1 shows the chemical structures of three CTAs used in this study. In this chapter, characterization data (SEC, ^{1}H NMR, DSC, TGA) of all the polymers synthesized with CTA1, CTA2 and CTA3 are represented in green (—), red (—) and blue (—) respectively. First, homopolymerization of styrene monomer was performed using all three CTAs following Scheme 2.1(1). Subsequently, the homopolymers were chain extended with vinylbenzyl chloride (VBC) monomer to form the diblock copolymer poly(S-*b*-VBC) (Scheme 2.1(2)). Monomer and initiator concentrations were investigated for chain extension polymerization with all three homopolymers (PS-CTA1, PS-CTA2, PS-CTA3).

2.4.1. Effect of CTA on Homopolymerization Reactions

Polystyrene homopolymerization reactions were executed using three different CTAs as shown in Scheme 2.1(1). All the reactions were performed in small scale (targeting 5 g yield) at 100 °C for 20 h with toluene as the solvent. The reactions were performed with a 1:100 mol:mol CTA:styrene ratio and a 1:1 wt:wt styrene:toluene ratio. The final polymer was obtained by twice precipitating the reaction mixture in methanol and subsequently drying the resulting polymer under dynamic vacuum in an oven at room temperature for 24 h.

Table 2.1 SEC molecular weight and dispersity for PS-CTAs.

Polymer	$\mathbf{M_{n,\,SEC}}$ **(kg/mol)**	$\boldsymbol{Đ}$
PS_{41}-CTA1	4.6	1.15
PS_{44}-CTA2	4.7	1.14
PS_{47}-CTA3	5.2	1.17

Figure 2.2 shows the SEC chromatograms of all three polystyrene homopolymers, each synthesized with a different CTA. The SEC chromatograms of three homopolymers overlap, indicating similar molecular weight and dispersity. The molecular weights and dispersities of all homopolymers are listed in Table 2.1.

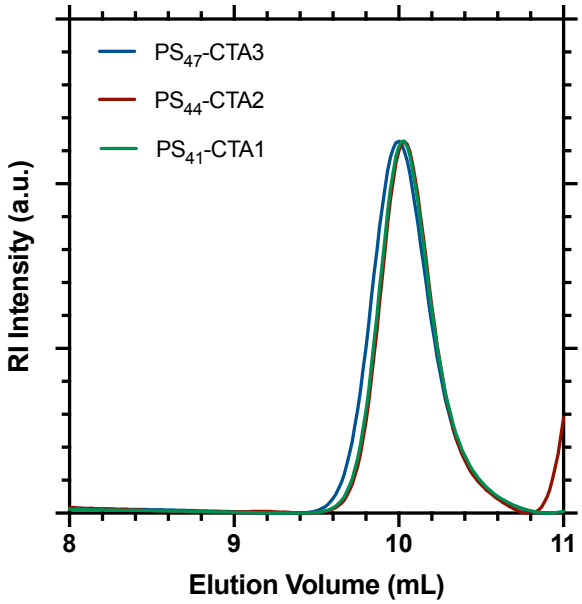

Figure 2.2 SEC chromatograms for PS-CTA1 (green), PS-CTA2 (red) and PS-CTA3 (blue).

Figure 2.3 shows ^{1}H NMR spectra of the three PS-CTAs, as well as the chemical structures and peak assignments. End group analysis for polymers made with CTA1 and CTA2 was not possible because of the absence of distinct end group peaks. For CTA3, end group peaks were clearly observed at 2.49 ppm and 2.19 ppm. Molecular weight of PS-CTA3 was calculated by using the integration ratio between the end group peak at 2.49 ppm (corresponds to 3H) and the broad polystyrene peak between 6.28 – 7.28 ppm. The molecular weight obtained from ^{1}H NMR (5.1 kg/mol) is in close agreement with SEC number average molecular weight (5.2 kg/mol).

$$^{1}\text{H NMR molecular weight} = \frac{\left(\frac{\text{aromatic protons peak}}{\text{peak (a)}}\right)}{\left(\frac{5}{3}\right)} \times (104.15) \qquad \textbf{(2.1)}$$

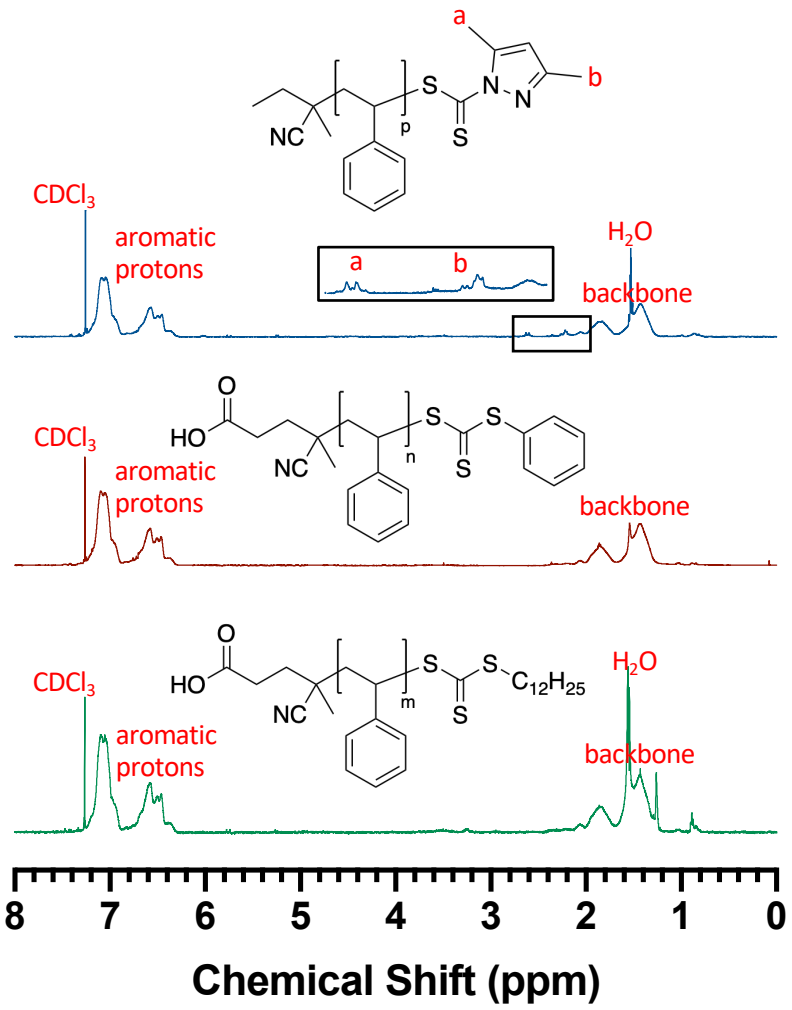

Figure 2.3 ^{1}H NMR spectra for PS-CTA1 (green), PS-CTA2 (red) and PS-CTA3 (blue).

Figure 2.4 shows the differential scanning calorimetry profiles for all three polystyrene homopolymers. The glass transition temperatures were determined using the midpoint method from the second thermogram heating cycle. The glass transition temperatures for PS-CTA1, PS-CTA2 and PS-CTA3 were 97 °C, 95 °C and 96 °C, respectively.

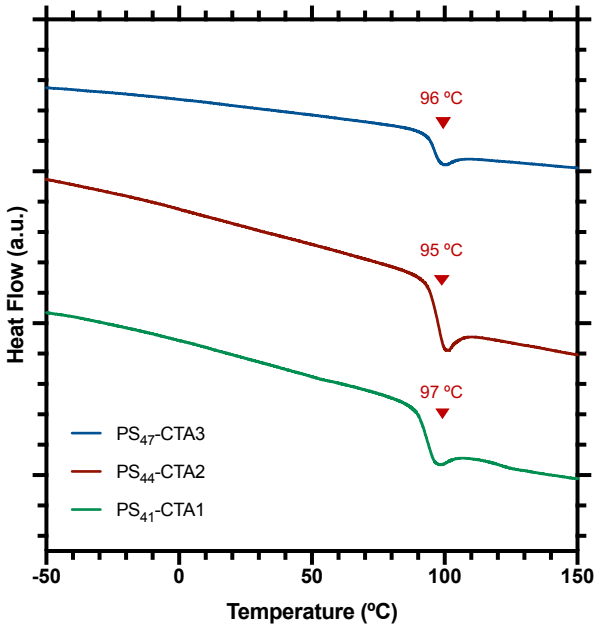

Figure 2.4 DSC profiles for PS-CTA1 (green), PS-CTA2 (red) and PS-CTA3 (blue).

Figure 2.5 shows the thermogravimetry profiles for all three polystyrene homopolymers. The degradation temperatures were determined at 5% weight loss. The degradation temperature for PS-CTA1, PS-CTA2 and PS-CTA3 were 318 °C, 323 °C and 325 °C, respectively.

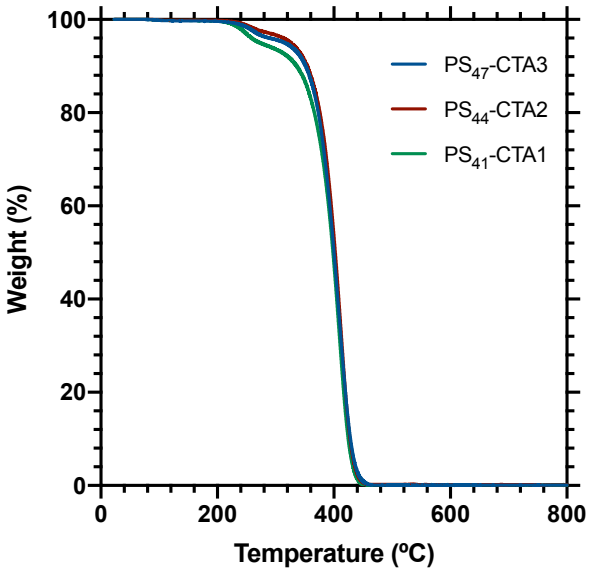

Figure 2.5 TGA profiles for PS-CTA1 (green), PS-CTA2 (red) and PS-CTA3 (blue).

Similar values of glass transition temperatures and thermal degradation temperatures among all three homopolymers corroborates that the thermal properties are a function of polymer molecular weight and polymer end groups do not have any significant impact on these properties.

2.4.2. Effect of CTA on Chain Extension Polymerization Reactions

Diblock copolymer poly(S-*b*-VBC) was synthesized by chain extension of polystyrene homopolymer (PS-CTA). The three different polystyrene homopolymers were chain extended with VBC as the monomer, AIBN as the initiator and THF as the solvent. The reactions were performed at 60 °C for 5 h with a 1.00:0.10 mol:mol ratio of PS-

CTA:AIBN initiator and a 1:1 wt:wt ratio of VBC:THF. Polymerizations were performed at different molar ratios of PS-CTA to VBC monomer (Table 2.2). The final polymer was obtained by twice precipitating the reaction mixture in methanol and drying under dynamic vacuum in an oven at room temperature for 24 h.

Table 2.2 SEC molecular weights and dispersities for poly (S-*b*-VBC) at various monomer ratios.

Polymer	**PS-CTA:VBC**[a]	$\mathbf{M_{n,\,SEC}}$ **(kg/mol)**	$\boldsymbol{Đ}$
Poly(S_{41}-*b*-VBC_{08})-CTA1	1:100	5.8	1.19
Poly(S_{41}-*b*-VBC_{47})-CTA1	1:200	11.8	1.45
Poly(S_{44}-*b*-VBC_{27})-CTA2	1:100	8.9	1.25
Poly(S_{44}-*b*-VBC_{31})-CTA2	1:200	9.5	1.55
Poly(S_{47}-*b*-VBC_{13})-CTA3	1:100	7.2	1.20
Poly(S_{47}-*b*-VBC_{26})-CTA3	1:200	9.2	1.25
Poly(S_{47}-*b*-VBC_{33})-CTA3	1:300	10.3	1.57

[a]mol:mol

Figure 2.6 shows the SEC chromatograms for chain extension polymerizations of PS-CTA1 and PS-CTA2. The dashed profile in each figure represents the corresponding precursor, PS-CTA1 and PS-CTA2, respectively. PS-CTA1 and PS-CTA2 chain extended

with well-defined molecular weights and low dispersities at high PS-CTA to monomer ratios (1:100 mol:mol). However, when monomer concentration was increased, *i.e.*, PS-CTA to monomer ratio decreased (1:200 mol:mol), the dispersities increased from 1.19 to 1.45 and 1.25 to 1.55, for PS-CTA1 and PS-CTA2 based diblock copolymers, respectively (see Table 2.2). This may be due to an inability of PS-CTA to efficiently control the polymerization at a low PS-CTA to monomer ratio (*i.e.*, high monomer concentration).

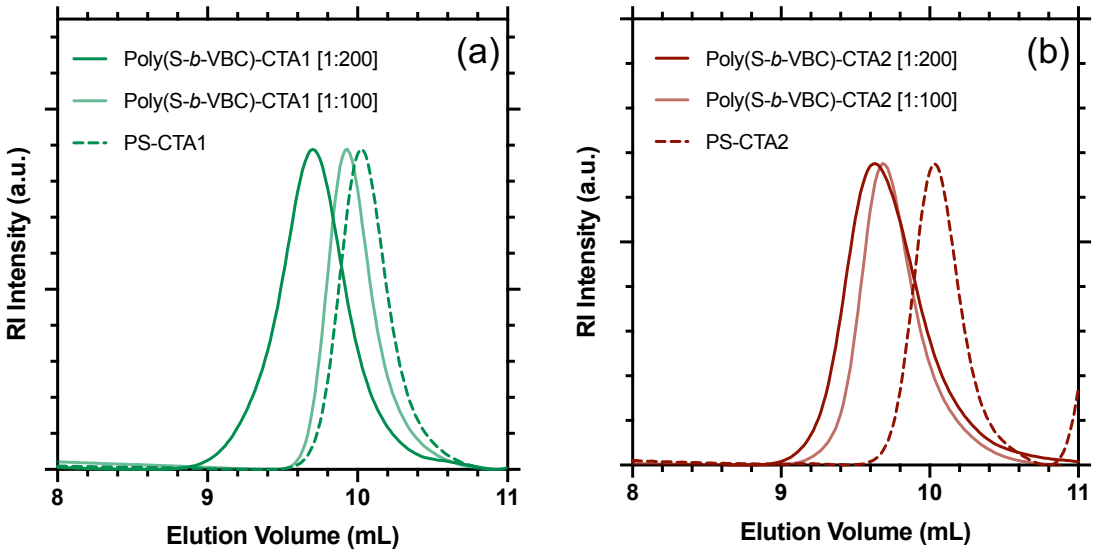

Figure 2.6 SEC chromatograms for diblock copolymer poly(S-*b*-VBC) at different monomer ratios chain extended from (a) PS-CTA1 (b) PS-CTA2.

Figure 2.7 shows the SEC chromatogram for chain extension polymerization of PS-CTA3. Chain extending PS-CTA3 resulted in block copolymers with well-defined molecular weights and dispersity for 1:100 mol:mol and 1:200 mol:mol of PS-CTA3:VBC, indicating CTA3 exhibits more exquisite control in chain extending VBC at these molar ratios compared to using CTA1 and CTA2 (see Table 2.2). Further increasing the molar ratio to 1:300 mol:mol PS-CTA3:VBC resulted in an increase in dispersity from 1.25 to 1.57, indicating loss in control at even lower PS-CTA to monomer ratio (*i.e.*, higher monomer concentration).

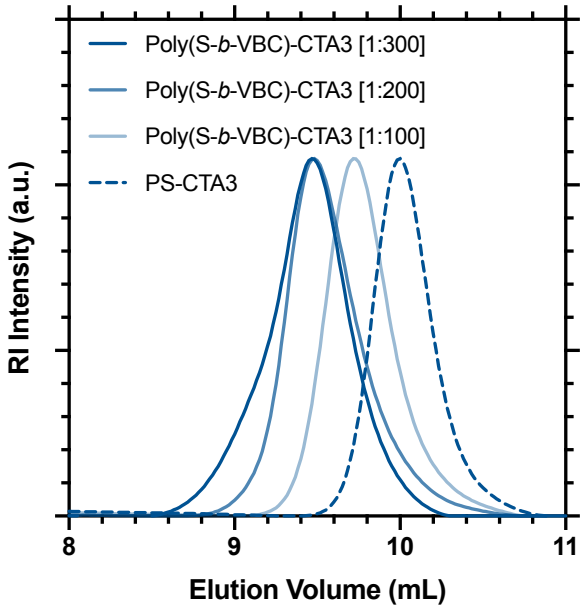

Figure 2.7 SEC profiles for poly(S-*b*-VBC) at different monomer ratios chain extended from PS-CTA3.

2.4.3. Effect of Initiator Concentration on Poly(S-*b*-VBC) Polymerization

The effect of AIBN initiator was studied at three molar ratios of PS-CTA3:initiator (Table 2.3). Chain extension of PS-CTA3 was performed with VBC monomer at 1.00:0.05 mol:mol, 1.00:0.10 mol:mol, and 1.00:0.20 mol:mol ratios of PS-CTA3:AIBN. Following Scheme 2.1(2), the reactions were executed at 60 °C for 5 h in THF. The final polymer was obtained by twice precipitating the reaction mixture in methanol and subsequently drying the resulting polymer under dynamic vacuum in an oven at room temperature for 24 h.

Table 2.3 SEC molecular weights and dispersities for poly (S-*b*-VBC) at different initiator ratios.

Polymer	**PS-CTA:VBC:AIBN**[a]	$\mathbf{M_{n,\,SEC}}$ **(kg/mol)**	***Đ***
Poly(S_{47}-*b*-VBC_{02})-CTA3	1.00:100.00:0.05	5.5	1.18
Poly(S_{47}-*b*-VBC_{13})-CTA3	1.00:100.00:0.10	7.2	1.20
Poly(S_{47}-*b*-VBC_{10})-CTA3	1.00:100.00:0.20	6.8	2.20

[a]mol:mol:mol

Figure 2.8 shows the SEC chromatograms for all the diblock copolymers, where the dashed profile represents the SEC chromatogram for PS-CTA3. Increasing the initiator ratio from 1.00:0.05 mol:mol to 1.00:0.10 mol:mol increased the monomer conversion

from 2% to 13%, while maintaining low dispersity. However, further increasing the initiator ratio to 1.00:0.20 mol:mol resulted in a non-uniform SEC chromatogram shown by the existence of two overlapping peaks in Figure 2.8. Increasing the amount of initiator increases the free radical generation at the start of reaction, which if not effectively controlled by the PS-CTA, can result in side reactions, such as homopolymerization of the VBC monomer.

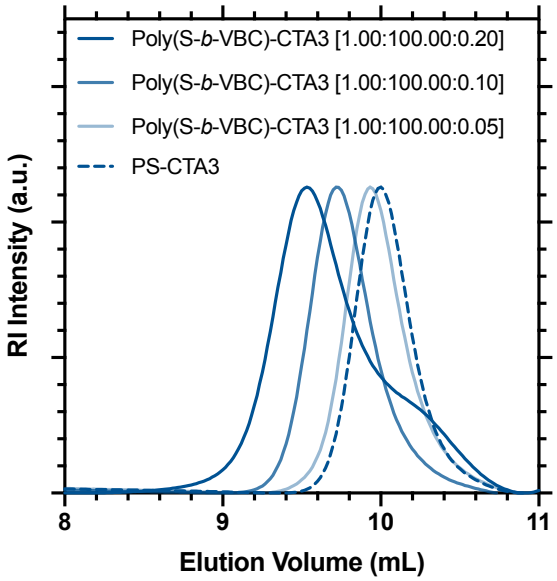

Figure 2.8 SEC chromatograms for poly(S-*b*-VBC) at different initiator ratios.

2.4.4. Scale-up Synthesis of Diblock Copolymer Poly(S-*b*-VBC)

The effect of reaction time was studied for polystyrene homopolymerization and chain extension reactions. The homopolymerization reactions were performed at a larger scale

(targeting 125 g yield) with CTA3 as the chain transfer agent, styrene as the monomer, and toluene as the solvent. This reaction was performed under reflux to help maintain ideal mixing. Reacting mixture aliquots were collected at the following fixed time intervals (4, 8, 12 and 22 h) and analyzed by SEC.

Figure 2.9 shows the SEC chromatograms for the polystyrene homopolymer at each time point (each aliquot). As reaction time increased, the SEC profiles shifted to earlier elution volumes, indicating an increase in polymer molecular weight and the successful addition of styrene repeat units to the polymer chain. The chromatograms show uniform polymer molecular weight distribution (dispersity < 1.2 for homopolymer) at all reaction times.

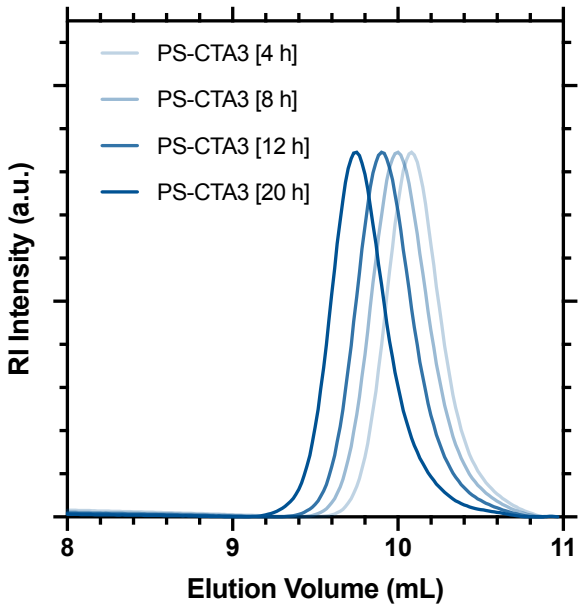

Figure 2.9 SEC chromatograms for PS-CTA3 at different reaction times.

The chain extension reaction was performed at a larger scale (targeting 50 g of final product) with PS-CTA3 as chain transfer agent, vinylbenzyl chloride as the monomer, AIBN as initiator, and THF as the solvent. The reaction was executed at reflux and aliquots were collected at specified time intervals (4, 8, and 12 h). Figure 2.10 shows the SEC chromatograms for the diblock copolymers at each time point (each aliquot). At 4 h, a diblock copolymer with a narrow dispersity (dispersity < 1.30) was obtained. Increasing the reaction time to 8 h did not result in a significant increase in molecular weight or dispersity. Further increasing the reaction time to 12 h resulted in a side reaction (VBC homopolymerization) as evidenced by the emergence of second SEC peak at an elution volume of 10.2 – 11.0 mL in Figure 2.10 (THF solvent peak appears after 11mL elution volume).

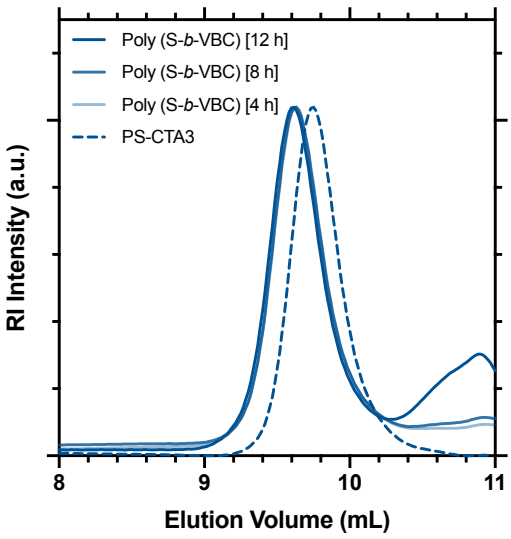

Figure 2.10 SEC chromatograms for poly(S-*b*-VBC) at different reaction times.

Figure 2.11(a) shows the ^{1}H NMR profile for polystyrene homopolymer (at 20 h). The aromatic proton peaks appear at 6.18 – 7.28 ppm and end group peaks appear at 2.49 ppm and 2.19 ppm. Other end group peaks appear along with backbone peaks between 2.14 – 1.16 ppm. The molecular weight of PS-CTA3 was calculated by using the integration ratio between the end group peak at 2.49 ppm and the broad polystyrene peak at 6.18 – 7.28 ppm using Equation 2.1. The molecular weight obtained from ^{1}H NMR (5.2 kg/mol) is in close agreement with SEC number average molecular weight (5.3 kg/mol).

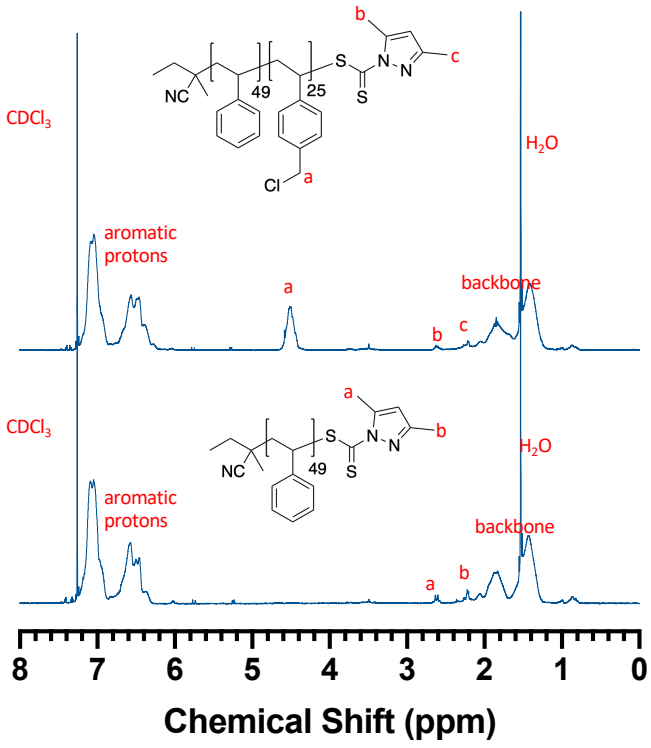

Figure 2.11 ^{1}H NMR spectra for (a) PS-CTA3 (b) poly(S-*b*-VBC).

Figure 2.11(b) shows the ^{1}H NMR spectra for poly(S-*b*-VBC) (at 5 h). The aromatic proton peaks appear between 6.28 – 7.28 ppm and emergence of peak at 4.67 – 4.29 ppm corresponds to the protons on the -C*H*$_2$Cl group of the vinylbenzyl chloride block. The molecular weight of poly(S-*b*-VBC) was calculated using the integration ratio between peak at 4.67 – 4.29 ppm and broad aromatic proton peak at 7.28 – 6.28 ppm. The molecular weight obtained from ^{1}H NMR (9.1 kg/mol) was higher than the SEC molecular weight (7.6 kg/mol). The lower molecular weight from SEC analysis may be a result of interactions of the -CH$_2$*Cl* group on the diblock copolymer with the Styragel GPC column.

2.4.5. Cost Analysis for Homopolymer Synthesis

Scaling up polymer synthesis can be more time efficient and cost effective. In this section, analysis of synthesis cost is presented by taking into consideration two major costs: materials and personnel time.

$$\text{Cost of synthesis} = \sum \text{Cost of material} + \sum \text{Cost of personnel time}$$

2.4.5.1. Material Costs

Table 2.4 presents materials cost for synthesizing polystyrene homopolymer at 5 g and 125 g scales, respectively. First, the cost of all the chemicals were estimated in US dollar ($) amounts per g (values based on quotations from vendors). These values were then multiplied by the amount of material utilized in the reaction. The total material costs

for each scale were determined by calculating the total sum. Finally, the normalized material cost was calculated by dividing the total material cost by amount of polymer synthesized in each reaction. The normalized material cost for reactions at the two different size scales do not differ significantly.

Table 2.4 Normalized material cost for polystyrene synthesis.

Material	**Price ($ / g)**	**Cost of Material in 5 g Scale ($)[a]**	**Cost of Material in 125 g Scale ($)[b]**
Styrene (S4972–1L)	0.049	0.49	12.28
Toluene (244511–1L)	0.072	0.72	18.01
CTA3 (BM1542– 5G)	30	7.31	182.56
THF (401757–2L)	0.099	0.99	39.60
Methanol (322415–4X4L)	0.003	0.36	15.00
Total material cost ($)		9.87	267.45
Yield (g)		4.72	120.48
Normalized material cost ($/g)[c]		**2.09**	**2.21**

[a]Based on material amount described in Section 2.2.1
[b]Based on material amount described in Section 2.2.2
[c]Normalized Material Cost ($ / g) = $\frac{\text{Total Material Cost (\$)}}{\text{Polymer Yield (g)}}$

2.4.5.2. Cost of Personnel Time

Table 2.5 presents the cost of personnel time for synthesizing polystyrene homopolymer. The total time, including preparation, synthesis and purification was determined for each scale. Cost of personnel time per hour was assumed \$25/h for reaction at each scale. Finally, normalized cost of personnel time was determined by calculating the ratio of total cost of personnel time to the amount of material synthesized at each scale.

Table 2.5 Normalized cost of personnel time for polystyrene synthesis.

Experimental Procedure	**5 g Scale Reaction**	**125 g Scale Reaction**
Preparation time (h)	2	4
Reaction time (h)[a]	2	2
Purification time (h)	2	8
Total time (h)	6	14
Personnel time cost (\$)	150	350
Normalized personnel time cost (\$/g)[b]	**31.77**	**2.90**

[a]Based on time spent by personnel monitoring the reaction. The reaction itself lasts 20 hours, but personnel time is not consumed for entire 20 h.

[b]Normalized cost of lab worker time (\$ / g) = $\frac{\text{Cost of Lab Worker Time (\$)}}{\text{Polymer Yield (g)}}$

The normalized material cost at both scales is similar, however, the normalized personnel time cost at 125 g scale is 11 times less expensive than normalized personnel time cost at 5 g scale. This is due to much larger production volume in similar time frame.

Table 2.6 Total normalized cost for polystyrene synthesis.

Cost	**5 g Scale Reaction**	**125 g Scale Reaction**
Normalized material cost ($/g)	2.09	2.21
Normalized cost of time ($/g)	31.77	2.90
Normalized total cost ($/g)	**33.86**	**5.11**

Overall, it can be concluded that total normalized cost (see Table 2.6) of synthesizing polystyrene (combination of material cost and cost of time) at a larger scale is around 7 times less expensive.

2.5. Conclusions

In this study, RAFT polymerization of styrene monomer and chain extension of polystyrene homopolymer with vinylbenzyl chloride monomer was investigated. Three CTAs were employed to investigated the impact on molecular weight and dispersity. For the homopolymerization reactions, no significant difference on molecular weight and

thermal analysis was observed between three CTAs. However, for chain extension polymerization reactions, CTA3 can result in diblock copolymers with narrow molecular weight distribution for wider range of monomer concentrations. Furthermore, CTA3 allows for molecular weight analysis of polymer using ^{1}H NMR spectroscopy due to presence of distinct end group peaks. Once the optimum conditions were determined in small scale (*ca.* 1 g product), the polystyrene homopolymer and poly(styrene-*b*-vinylbenzyl chloride) [poly(S-*b*-VBC)] synthesis was scaled up and effect of time was reported. It was concluded that PS-CTA3 can polymerize for an extended period of time, resulting in polymers with well-defined molecular weight. However, side reactions (such as VBC homopolymerization) can occur during poly(S-*b*-VBC) synthesis after 8 h of polymerization time. Finally, cost analysis for scaling up the homopolymer synthesis was reported and it was concluded that synthesizing polystyrene at 125 g scale is 7 times less expensive than synthesizing polystyrene at 5 g scale.

3. SYNTHESIS OF POLYMERIZED IONIC LIQUID TRIBLOCK TERPOLYMER POLY(STYRENE-*B*-VINYLBENZYL METHYLPYRROLIDINIUM CHLORIDE-*B*-OCTYLSTYRENE)

3.1. Introduction

In the previous section, the diblock copolymer poly(styrene-*b*-vinylbenzyl chloride) was synthesized at a 50 g scale. In this study, a reaction scheme was developed to further chain extend the diblock copolymer and obtain a triblock terpolymer. This triblock terpolymer was subsequently functionalized to obtain a PIL triblock terpolymer.

Many common chain transfer agents (CTAs) used in reversible addition-fragmentation chain-transfer (RAFT) polymerization are capable of polymerizing styrenes, acrylates, acrylamides, methacrylates, methacrylamides, vinyl esters, and vinyl amides. However, all of these monomer types, except styrene, can undergo chemical degradation in the strong alkaline environment of AFCs.[17, 55] Hence a styrene-based monomer would be a more appropriate choice. Matsushima *et. al.*[56] demonstrated that adding long alkyl chain to styrene (resulting in alkylstyrene), the glass transition temperature for corresponding polymer can be decreased significantly. For example, a homopolymer made from 4-octylstyrene monomer (number average molecular weight 11 kg/mol) has a glass transition temperature of –30 °C. Therefore, 4-octylstyrene was used as the third block in this study to add a block that is both highly chemically stable and flexible.

3.2. Experimental Method

3.2.1. Materials

2-cyanobutanyl-2-yl 3,5-dimethyl-1H-pyrazole-1-carbodithioate (chain transfer agent (CTA3), ≥95%) was used as received from Boron Molecular. Toluene (anhydrous, 99.8%), methanol (ACS Reagent, ≥99.8%,), tetrahydrofuran (THF, ≥99.9%), inhibitor removers (for removing tert-butylcatechol), tetrahydrofuran (HPLC THF, HPLC grade, ≥99.9%), chloroform-d (100%, 99.96 atom %D) and *N*-methylpyrrolidine (NMP, 97%) were used as received from Sigma Aldrich. 4-vinylbenzyl chloride (90%, contains 500 ppm 4-tert-butylcatechol as stabilizer), and styrene (ReagentPlus, contains 4-tert-butylcatechol as stabilizer, ≥99%) were purchased from Sigma Aldrich and purified by passing through aluminum oxide column before use. Azobis(isobutyronitrile) (AIBN, 98%, Sigma Aldrich) and 1,1'-Azobis(cyanocyclohexane) (ACHN, 98%, Sigma Aldrich) were purified by recrystallization twice from methanol. 4-octylstyrene (≥95%, contains tert-butylcatechol) was purchased from TCI Chemicals and purified by passing through an aluminum oxide column before use.

3.2.2. Synthesis of PS-CTA3

PS-CTA3 was synthesized as described in Section 2.2.3.

3.2.3. Synthesis of Poly(S-*b*-VBC)

Poly(S-*b*-VBC) was synthesized as described in Section 2.2.5.

3.2.4. Synthesis of Poly(S-*b*-VBC-*b*-OS)

The triblock terpolymer poly(styrene-*b*-vinylbenzyl chloride-*b*-octylstyrene) [poly(S-*b*-VBC-*b*-OS] was synthesized by chain extension of diblock copolymer poly(S-*b*-VBC) (Scheme 3.1(3)). 1.8 g of poly(S-*b*-VBC), 5.14 g of purified (by passing through aluminum oxide column) 4-octylstyrene, 0.0028 g of ACHN and 5.10 g of toluene were mixed in a 25 mL Schlenk flask. The flask was subjected to four freeze-pump-thaw degassing cycles followed by sealing the reactor and performing the reaction under static nitrogen at 100 °C for 22 h. The resulting polymer was twice precipitated in methanol and dried under dynamic vacuum in an oven at room temperature for 24 h. Yield: 2.42 g of solid particles. ^{1}H NMR (500 MHz, $CDCl_3$, 23 °C) δ (ppm): 7.28-6.18 (m, 13H, C_6H_5, C_6H_4-CH_2, C_6H_4- C_8H_{17}), 4.67-4.29 (s, 2H, C_6H_4-CH_2), 2.67-2.32 (s, 2H, C_6H_4-CH_2-C_7H_{15}), 2.32-1.04 (m, 21H, CH_2-CH, CH_2-CH, C_6H_4-CH_2-CH_2-C_5H_{10}-CH_3), 0.95-0.74 (s, 3H, C_6H_4-C_7H_{14}-CH_3) (Figure 3.2); SEC (THF, 40 °C): M_n = 10.4 kg mol^{-1}, M_w/M_n = 1.32 (against PS standards) (Figure 3.1).

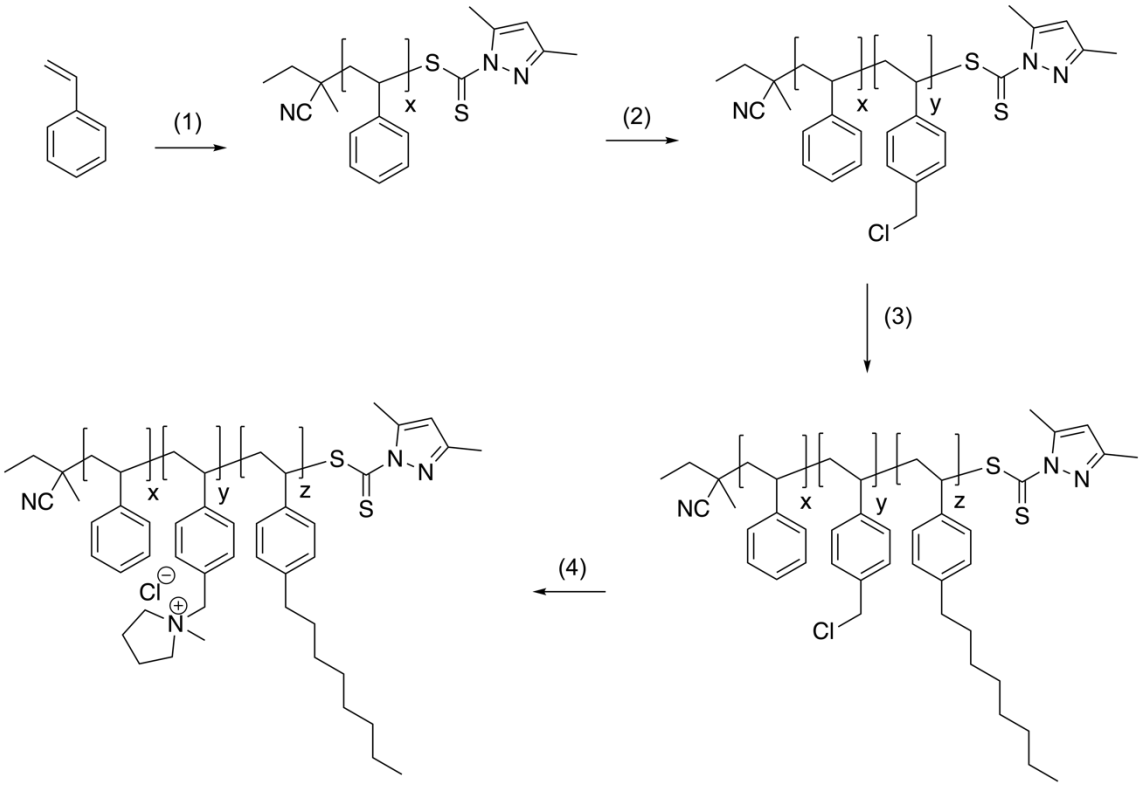

(1) CTA, Toluene, 20 h, reflux; (2) VBC, AIBN, THF, 5 h, reflux;
(3) OS, ACHN, 22 h, 100 ºC; (4) *N*-methylpyrrolidine, DMF, 48 h, 80 ºC

Scheme 3.1 Polymerization of (1) polystyrene, (2) poly(styrene-*b*-vinylbenzyl chloride), (3) poly(styrene-*b*-vinylbenzyl chloride-*b*-octylstyrene) and (4) poly(styrene-*b*-vinylbenzyl methylpyrrolidinium chloride-*b*-octylstyrene)

3.2.5. Synthesis of Poly(S-*b*-VBMPyr-Cl-*b*-OS)

Triblock terpolymer poly(S-*b*-VBC-*b*-OS) was functionalized using NMP to obtain poly(styrene-*b*-vinylbenzyl methylpyrrolidinium chloride-*b*-octylstyrene) [poly(S-*b*-

VBMPyr-Cl-*b*-OS)] (Scheme 3.1(4)). 1.5 g of poly(S-*b*-VBC-*b*-OS), 0.935 g of NMP and 6 mL of DMF were mixed together in a 20 mL vial. The vial was sealed, and the reaction was performed by placing the vial in an oil bath at 80 °C for 48 h. The resulting polymer was extensively washed with hexane, then extensively washed with acetone, and then dried under vacuum in an oven at room temperature for 24 hrs. Yield: 1.62 g of solid particles. ^{1}H NMR (500 MHz, $CDCl_3$, 23 °C) δ (ppm): 7.30-6.03 (m, 13H, C_6H_5, C_6H_4-CH_2, C_6H_4- C_8H_{17}), 4.29-3.77 (s, 2H, C_6H_4-CH_2-N), 3.79-3.32 (m, 4H, N-CH_2-CH_2-CH_2-CH_2-N), 3.33-2.83 (m, 4H, N-CH_2-CH_2-CH_2-CH_2-N), 2.58-2.30 (s, 2H, C_6H_4-CH_2-C_7H_{15}), 2.30-2.09 ppm (N-CH_3), 2.09-0.96 ppm (m, 21H, CH_2-CH, CH_2-CH, C_6H_4-CH_2-CH_2-C_5H_{10}-CH_3), 0.95-0.69 (s, 3H, C_6H_4-C_7H_{14}-CH_3) (Figure 3.3).

3.3. Characterization

Molecular weights and molecular weight distributions of PS-CTA3, poly(S-*b*-VBC) and poly(S-*b*-VBC-*b*-OS) were determined by size exclusion chromatography (SEC) using Waters Gel Permeation Chromatography (GPC) system equipped with a THF Styragel column (Styragel@HR 5E, effective separation of molecular weight range: 2-4000 kg mol^{-1}) and a 2414 refractive index (RI) detector. All measurements were performed at 40 °C. HPLC THF was used as the mobile phase at a flow rate of 1.0 mL/min. PS standards (Shodex, Japan) with molecular weights ranging from 2.97 to 983 kg mol^{-1} were used for calibration.

Chemical structures and number-average molecular weights of PS-CTA3, poly(S-*b*-VBC) and poly(S-*b*-VBC-*b*-OS) and poly(S-*b*-VBMPyr-Cl-*b*-OS) were characterized by ^{1}H NMR spectroscopy using a Varian 500 MHz spectrometer at 23 °C with $CDCl_3$ as the solvent. All chemical peaks were referenced to chloroform peak ($CHCl_3$) at 7.27 ppm.

Glass transition temperature (T_g) was determined by differential scanning calorimetry (DSC; TA Instruments, Q200) over a temperature range of –140 °C to 200 °C at a heating/cooling rate of 10 °C/min under a nitrogen environment (50 mL/min) using a heat/cool/heat method. T_g was determined using the midpoint method from the second thermogram heating cycle.

Thermal degradation temperature (T_d) were determined using thermogravimetry analysis (TGA; TA Instruments, Q50) over a temperature range of 25 °C to 900 °C at a heating rate of 10 °C/min under a nitrogen environment (60 mL/min). The degradation temperature was determined at 5% weight loss.

Small-angle X-ray scattering (SAXS) data for poly(S-*b*-VBC) and poly(S-*b*-VBC-*b*-OS) and poly(S-*b*-VBMPyr-Cl-*b*-OS) were collected using a Rigaku SMAX-3000 instrument. A rotating copper anode (MicroMax-007HFM, Rigaku) operated at 40 kV and 30 mA was used to generate characteristic Cu X-rays with a wavelength (λ) of 1.542 Å. The X-rays were focused, monochromated, and collimated using a Confocal Max-Flux double-focusing optic and subsequent pinhole collimation. The samples were characterized at a sample-to-detector distance of 1.5 m using a Gabriel-type 2D multi-wire detector. Distance calibrations were performed using silver behenate. SAXS data was

collected under vacuum at room temperature with exposure times ranging from 900 to 1800 s. The raw data were corrected for transmission and background noise, then averaged azimuthally to give intensity as a function of momentum transfer magnitude, I(q), where $q = 4\pi (\sin \theta)/\lambda$ and 2θ is the scattering angle. The q range was from 0.007 $Å^{-1}$ to 0.300 $Å^{-1}$. The intensities were reported in arbitrary units (a.u.).

3.4. Results and Discussions

A triblock terpolymer (TTP) was synthesized as shown in Scheme 3.1 (3). To synthesize this TTP, chain extension of diblock copolymer [poly(S-*b*-VBC)] was performed using RAFT polymerization. The synthesized TTP was subsequently functionalized with a pyrrolidinium based cation and the thermal properties were analyzed using DSC and TGA.

Figure 3.1 shows the SEC chromatograms for polystyrene homopolymer, PS-CTA3, poly(S-*b*-VBC) and poly(S-*b*-VBC-*b*-OS). A successful chain extension of homopolymer and diblock copolymer is evident, as the SEC chromatogram shifts to lower elution time, indicating an increase in molecular weight. The narrow breath of all three chromatograms signifies low dispersities. Table 3.1 shows the SEC number average molecular weight and dispersity of all the three polymers: PS-CTA3, poly(S-*b*-VBC) and poly(S-*b*-VBC-*b*-OS).

Table 3.1 Molecular weight and dispersity of PS-CTA3, poly(S-*b*-VBC) and poly(S-*b*-VBC-*b*-OS).

Polymer	**$M_{n,\,SEC}$ (kg/mol)**	***Đ***	**$M_{n,\,NMR}$ (kg/mol)**
PS_{49}-CTA3[a]	5.3	1.18	5.3
Poly(S_{49}-*b*-VBC_{25})[a]	7.6	1.29	9.1
Poly(S_{49}-*b*-VBC_{25}-*b*-OS_{29})[a]	10.4	1.32	15.4

[a]number of repeat units based on ^{1}H NMR molecular weight analysis

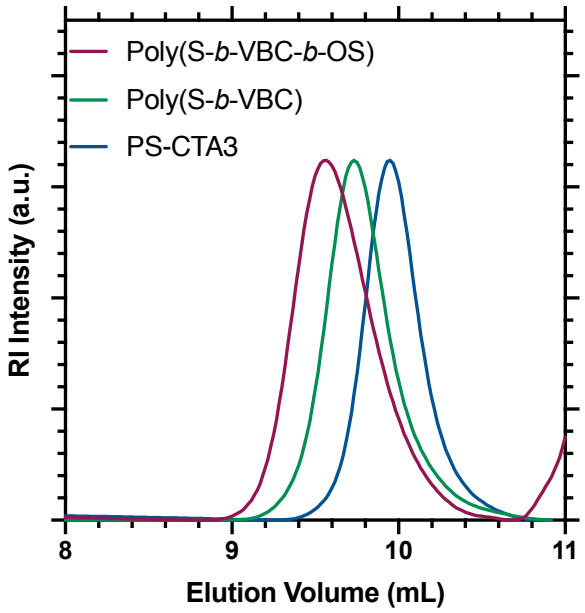

Figure 3.1 SEC chromatograms for PS-CTA3 (blue), poly(S-*b*-VBC) (green), poly(S-*b*-VBC-*b*-OS) (red).

Figure 3.2 shows ^{1}H NMR spectra for the chain extension of poly(S-*b*-VBC) resulting in the formation of the triblock terpolymer poly(S-*b*-VBC-*b*-OS). In addition to peaks corresponding to diblock copolymer, new peaks emerge between 2.67 – 2.32 ppm and between 0.95 – 0.74 ppm, which corresponds to protons on long alkyl side chain on 4-octylstyrene block. Other proton peaks appear between 2.32 – 1.04 ppm along with polymer backbone peaks. The ratio of integration between peak d (2.67 – 2.32 ppm) and peak c (4.67 – 4.29 ppm) was used to calculate number averaged molecular weight for poly(S-*b*-VBC-*b*-OS).

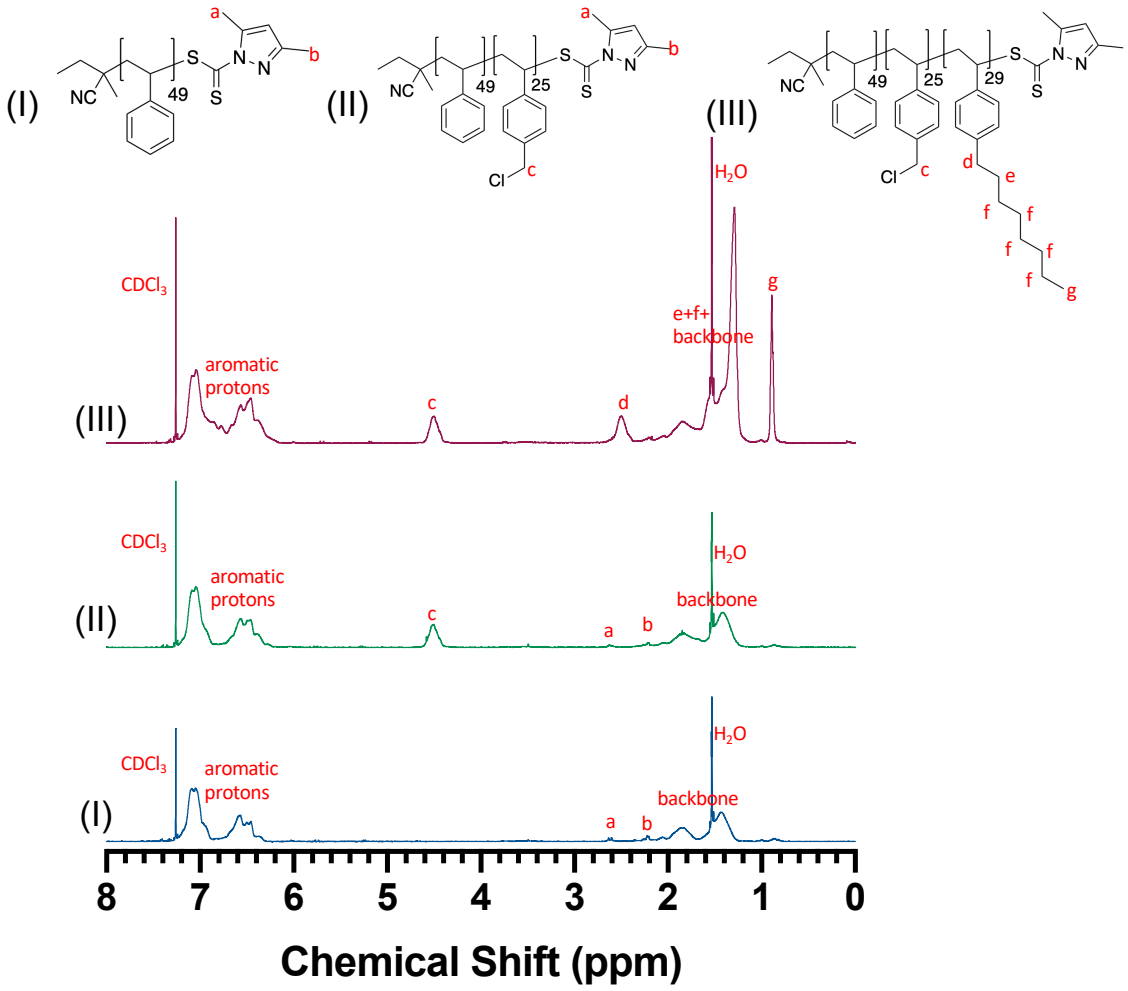

Figure 3.2 ^{1}H NMR spectra for poly(S-*b*-VBC-*b*-OS) (red), poly(S-*b*-VBC) (green) and PS-CTA3 (blue).

Figure 3.3 shows the ^{1}H NMR spectra for functionalization of poly(S-*b*-VBC-*b*-OS) resulting in formation of poly(S-*b*-VBMPyr-Cl-*b*-OS). The aromatic proton peaks appear between 7.30 – 6.03 ppm and peaks corresponding to protons on cation ring appear

between 3.79 – 3.32 ppm, 3.33 – 2.83 and 2.30 – 2.09 ppm. The peaks corresponding to long alkyl chain on 4-octylstyrene block appear between 2.58 – 2.30 ppm and 2.09 – 0.96 ppm along with polymer backbone peaks. The degree of functionalization can be calculated using equation 3.1. The integration ratio of 1.49:1 between peaks h (2.30 – 2.09 ppm) and peak a (4.29 – 3.77 ppm) indicates greater than 99% functionalized polymer.

$$degree\ of\ functionalizatio = \frac{\left(\frac{peak\ (h)}{peak\ (a)}\right)}{\left(\frac{3}{2}\right)} \quad \textbf{(3.1)}$$

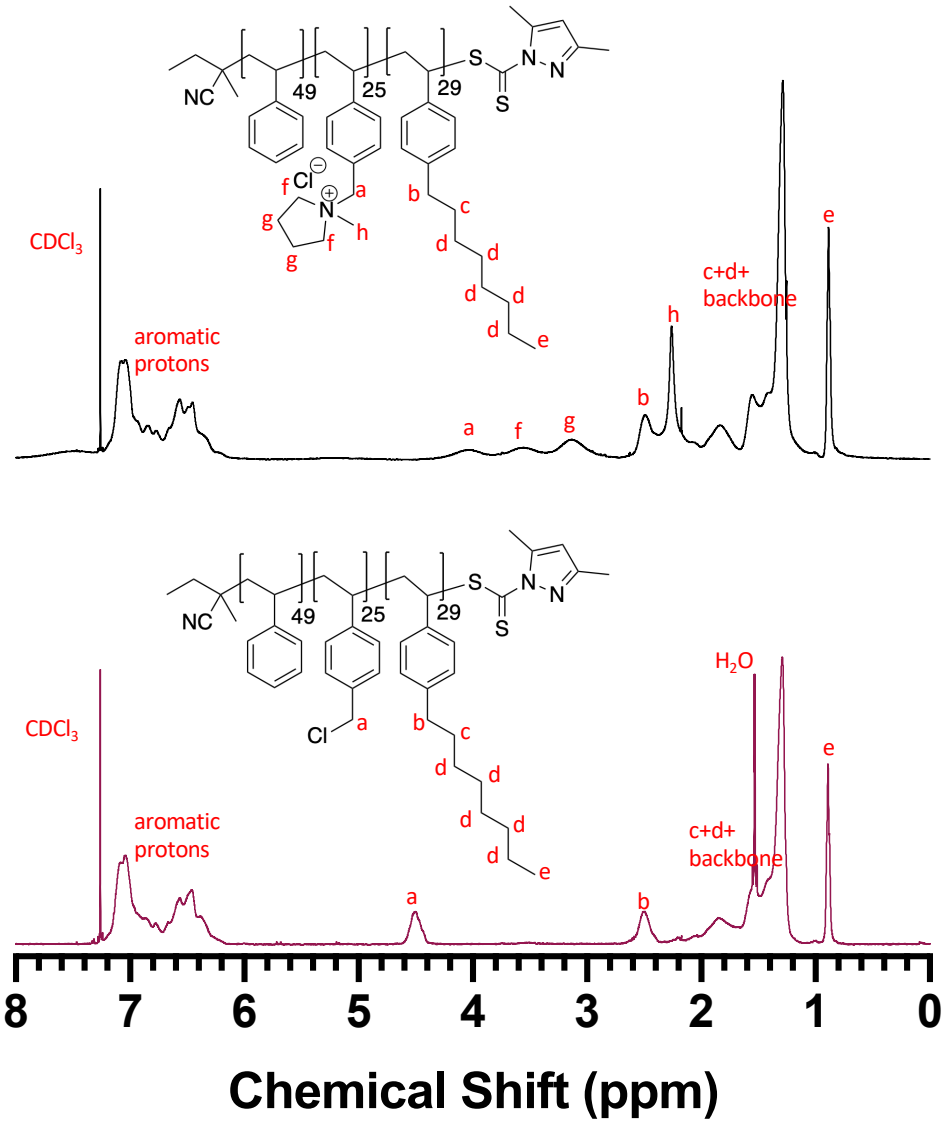

Figure 3.3 ^{1}H NMR spectra for poly(S-*b*-VBMPyr-Cl-*b*-OS) (black) and poly(S-*b*-VBC-*b*-OS) (red).

Figure 3.4 shows differential scanning calorimetry profiles for PS-CTA3, poly(S-*b*-VBC), poly(S-*b*-VBC-*b*-OS) and poly(S-*b*-VBMPyr-Cl-*b*-OS). Polystyrene

homopolymer and poly(S-*b*-VBC) revealed single glass transition temperatures at 96 °C and 99 °C, respectively. However, the addition of a third block resulted in presence of two glass transition temperatures, indicating the presence of phase separation. The lower glass transition temperature appears at –22 °C corresponding to poly(octylstyrene) block. The higher glass transition temperature is located at 82 °C. This higher T_g could be a result of certain degree of phase mixing between the polystyrene backbones of the three blocks, resulting in a slight decrease in the T_g [compared to the T_g of polystyrene block]. The functionalized triblock terpolymer poly(S-*b*-VBMPyr-Cl-*b*-OS) revealed a single glass transition temperature at 101 °C.

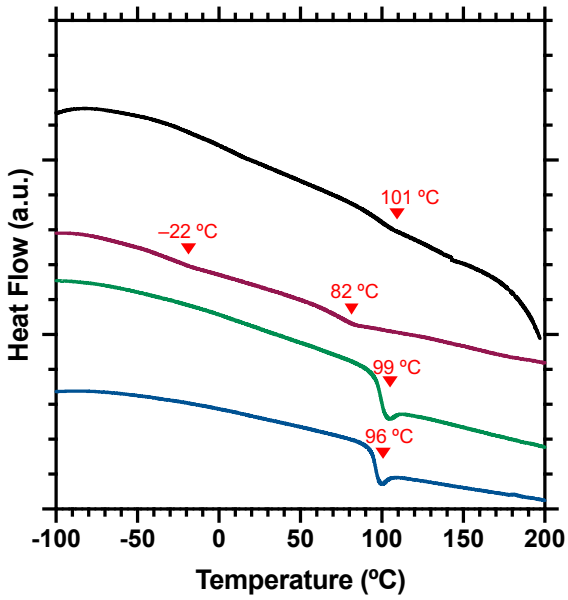

Figure 3.4 DSC profiles for PS-CTA3 (blue), poly(S-*b*-VBC) (green), poly(S-*b*-VBC-*b*-OS) (red), poly(S-*b*-VBMPyr-Cl-*b*-OS) (black).

Figure 3.5 shows the thermogravimetry profiles for PS-CTA3, poly(S-*b*-VBC), poly(S-*b*-VBC-*b*-OS) and poly(S-*b*-VBMPyr-Cl-*b*-OS). PS-CTA3, poly(S-*b*-VBC), poly(S-*b*-VBC-*b*-OS) corresponding to degradation temperatures of 320 °C, 319 °C and 324 °C, respectively. The similarity in degradation temperatures may be possible due to the styrene based chemical structures of all three blocks. However, the functionalized triblock terpolymer, poly(S-*b*-VBMPyr-Cl-*b*-OS), has a degradation temperature of 225 °C, which may be initiated at an earlier temperature due to the onset of degradation of cyclic cation ring.[18]

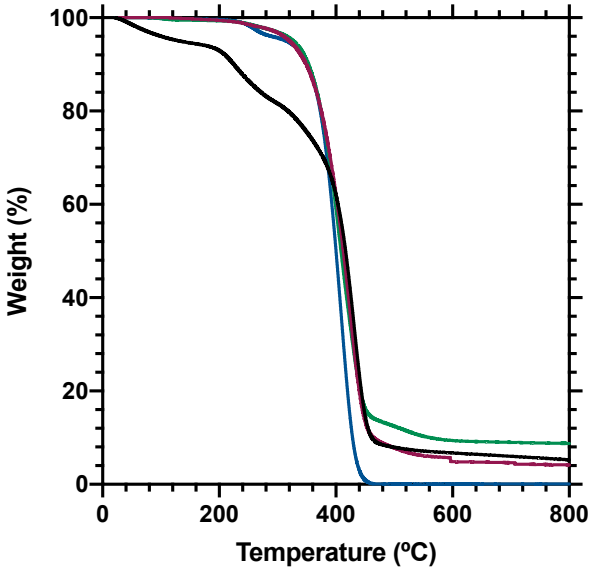

Figure 3.5 TGA profiles for PS-CTA3 (blue), poly(S-*b*-VBC) (green), poly(S-*b*-VBC-*b*-OS) (red), poly(S-*b*-VBMPyr-Cl-*b*-OS) (black).

Figure 3.6 shows the small angle X-ray scattering (SAXS) profiles for poly(S-*b*-VBC), poly(S-*b*-VBC-*b*-OS) and poly(S-*b*-VBMPyr-Cl-*b*-OS) (in powder form). The SAXS pattern for the functionalized triblock terpolymer poly(S-*b*-VBMPyr-Cl-*b*-OS) revealed two scattering peaks at q^* and $2q^*$, indicating the presence of an ordered microphase separation, possibly with lamellar morphology. The interdomain spacing was calculated as $d = 2\pi/q^* = 27.8$ nm. Further morphology analysis using transmission electron microscopy (TEM) is required to confirm the morphology type. Meanwhile, poly(S-*b*-VBC) and poly(S-*b*-VBC-*b*-OS) did not show presence of any peaks in the SAXS profile; this may be the result of the lack of significant electron density differences between the three styrene-based chemistries.

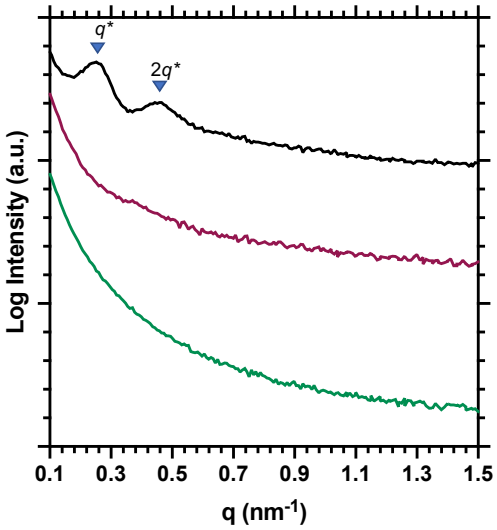

Figure 3.6 SAXS profile for functionalized triblock terpolymer poly(S-*b*-VBC) (green), poly(S-*b*-VBC-*b*-OS) (red), poly(S-*b*-VBMPyr-Cl-*b*-OS) (black) **(**in powder form).

3.5. Conclusions

In this study, a triblock terpolymer, poly(S-*b*-VBC-*b*-OS), was synthesized using RAFT polymerization. The chemical structure of the triblock terpolymer was determined using ^{1}H NMR and a low dispersity was confirmed using SEC. Thermal analysis of the triblock terpolymer revealed the presence of two glass transition temperatures at –22 °C and 82 °C, which indicates phase separation in the polymer. The thermal degradation for poly(S-*b*-VBC-*b*-OS) was observed at 324 °C, which is similar to the degradation temperature of the precursor diblock copolymer poly(S-*b*-VBC) (319 °C). The functionalized triblock terpolymer poly(S-*b*-VBMPyrl-Cl-*b*-OS) possessed a single glass transition temperature at 105 °C and a degradation temperature at 225 °C (may be due to the onset of degradation of the cyclic cation ring). SAXS analysis of the functionalized ionic triblock terpolymer revealed two scattering peaks, suggesting an ordered microphase separation, unlike the non-ionic triblock terpolymer, which did not show any scattering peaks, but this may be due to similar electron density of all the polymer block chemistries.

4. CONCLUSION AND FUTURE OUTLOOK

4.1. Summary

In this study, a diblock copolymer poly(styrene-*b*-vinylbenzyl chloride) [poly(S-*b*-VBC)] was synthesized using reversible addition-fragmentation chain-transfer (RAFT) polymerization and the effect of chain transfer agent (CTA), and monomer and initiator concentration were investigated in small scale (*ca.* 1 g product). First, three different CTAs (CTA1, CTA2 and CTA3) were employed to synthesize PS-CTA, which was subsequently chain extended using vinylbenzyl chloride (VBC) monomer to form the diblock copolymer poly(S-*b*-VBC). It was determined that PS-CTA3 can be used to synthesize diblock copolymers with narrow molecular weight distributions for a wider range of monomer concentrations. Furthermore, CTA3 allows for ^{1}H NMR based molecular weight analysis of PS-CTA3 and poly(S-*b*-VBC) polymers due to the presence of distinct end group peaks in the ^{1}H NMR spectra.

Once the optimum conditions were determined in small scale for poly(S-*b*-VBC) synthesis, the polystyrene homopolymer and poly(S-*b*-VBC) syntheses were scaled up to 125 g scale and 50 g scale, respectively. Cost analysis was performed for scaling up the polystyrene homopolymer synthesis and it was determined that synthesizing polystyrene at 125 g scale was 7 times less expensive than synthesizing polystyrene at 5 g scale.

The diblock copolymer poly(S-*b*-VBC) was further chain extended by adding 4-octylstyrene monomer as the third block. The chemical structure and molecular weight of the triblock terpolymer poly(styrene-*b*-vinylbenzyl chloride-*b*-octylstyrene)

[poly(S-*b*-VBC-*b*-OS)] was determined using ^{1}H NMR. Thermal studies using DSC revealed the presence of two glass transition temperatures in the triblock terpolymer poly(S-*b*-VBC-*b*-OS), indicating phase separation. Subsequently, the triblock terpolymer was functionalized using *N*-methylpyrrolidine to obtain an ionic PIL triblock terpolymer poly(styrene-*b*-vinylbenzyl methylpyrrolidinium chloride-*b*-octylstyrene). SAXS analysis of the functionalized triblock terpolymer (in powder form) revealed the presence of two scattering peaks, which suggests an ordered microphase separation due to differences in electron densities between the ionic and non-ionic blocks.

4.2. Future Directions

Multiple research directions and possibilities can be investigated in the future. The morphology diagram of ABC triblock terpolymer poly(styrene-*b*-vinylbenzyl methylpyrrolidinium chloride-*b*-octylstyrene) can be explored by synthesizing the polymer in various compositions (*i.e.,* volume fractions) of the three blocks. Various compositions can be synthesized by altering the reactions conditions (*e.g.,* temperature, initiator and monomer concentration). The ionic conductivity of polymers with different morphologies can be investigated to determine the ideal morphology for fuel cell applications.

Changing the order of block positions in the triblock terpolymer system can change the domain arrangement, which would result in additional morphologies for ACB and BAC

systems. RAFT polymerization allows for sequential addition of monomers. Therefore, by changing the reaction sequence, block position can be changed.

Finally, alkyl side chains (on the alkylstyrene block) of different lengths can be investigated for their effect on the physical properties, such as mechanical strength and toughness of the triblock terpolymers. Furthermore, the effects on morphology (and hence conductivity) can also be explored.

Overall, this study leaves a framework for future exploration of appropriate side chain length, block sequence and ideal composition for application of triblock terpolymers as membranes for AFCs.

REFERENCES

1. United States Environmental Protection Agency Overview of Greenhouse Gases. (accessed 01/10/2020).

2. Thomas, C. E., *International Journal of Hydrogen Energy* **2009,** *34* (15), 6005-6020.

3. Meek, K. M. Alkaline Chemical Stability and Ion Transport in Polymerized Ionic Liquid Anion Exchange Membranes. 2016.

4. Varcoe, J. R.; Slade, R. C. T., *Fuel Cells* **2005,** *5* (2), 187-200.

5. Merle, G.; Wessling, M.; Nijmeijer, K., *Journal of Membrane Science* **2011,** *377* (1-2), 1-35.

6. Nykaza, J. R.; Ye, Y. S.; Elabd, Y. A., *Polymer* **2014,** *55* (16), 3360-3369.

7. Ye, Y. S.; Elabd, Y. A., *Macromolecules* **2011,** *44* (21), 8494-8503.

8. Nunez, S. A.; Hickner, M. A., *Acs Macro Letters* **2013,** *2* (1), 49-52.

9. Tsai, T. H.; Maes, A. M.; Vandiver, M. A.; Versek, C.; Seifert, S.; Tuominen, M.; Liberatore, M. W.; Herring, A. M.; Coughlin, E. B., *Journal of Polymer Science Part B-Polymer Physics* **2013,** *51* (24), 1751-1760.

10. Vandiver, M. A.; Caire, B. R.; Poskin, Z.; Li, Y. F.; Seifert, S.; Knauss, D. M.; Herring, A. M.; Liberatore, M. W., *Journal of Applied Polymer Science* **2015,** *132* (10).

11. Yan, J. L.; Hickner, M. A., *Macromolecules* **2010,** *43* (5), 2349-2356.

12. Sturgeon, M. R.; Macomber, C. S.; Engtrakul, C.; Long, H.; Pivovar, B. S., *Journal of the Electrochemical Society* **2015,** *162* (4), F366-F372.

13. Choe, Y. K.; Fujimoto, C.; Lee, K. S.; Dalton, L. T.; Ayers, K.; Henson, N. J.; Kim, Y. S., *Chemistry of Materials* **2014,** *26* (19), 5675-5682.

14. Chen, D. Y.; Hickner, M. A., *Macromolecules* **2013,** *46* (23), 9270-9278.

15. Hibbs, M. R., *Journal of Polymer Science Part B-Polymer Physics* **2013,** *51* (24), 1736-1742.

16. Meek, K. M.; Elabd, Y. A., *Macromolecules* **2015,** *48* (19), 7071-7084.

17. Meek, K. M.; Nykaza, J. R.; Elabd, Y. A., *Macromolecules* **2016,** *49* (9), 3382-3394.

18. Sun, R.; Elabd, Y. A., *Acs Macro Letters* **2019,** *8* (5), 540-545.

19. Stancik, C. M.; Lavoie, A. R.; Achurra, P. A.; Waymouth, R. M.; Gast, A. P., *Langmuir* **2004,** *20* (21), 8975-8987.

20. Stancik, C. M.; Lavoie, A. R.; Schutz, J.; Achurra, P. A.; Lindner, P.; Gast, A. P.; Waymouth, R. M., *Langmuir* **2004,** *20* (3), 596-605.

21. Weber, R. L.; Ye, Y. S.; Schmitt, A. L.; Banik, S. M.; Elabd, Y. A.; Mahanthappa, M. K., *Macromolecules* **2011,** *44* (14), 5727-5735.

22. Cheng, S. J.; Beyer, F. L.; Mather, B. D.; Moore, R. B.; Long, T. E., *Macromolecules* **2011,** *44* (16), 6509-6517.

23. Green, M. D.; Wang, D.; Hemp, S. T.; Choi, J. H.; Winey, K. I.; Heflin, J. R.; Long, T. E., *Polymer* **2012,** *53* (17), 3677-3686.

24. Li, X.; Ni, X. F.; Liang, Z. H.; Shen, Z. Q., *Journal of Polymer Science Part a-Polymer Chemistry* **2012,** *50* (10), 2037-2044.

25. Karjalainen, E.; Khlebnikov, V.; Korpi, A.; Hirvonen, S. P.; Hietala, S.; Aseyev, V.; Tenhu, H., *Polymer* **2015,** *58*, 180-188.

26. Texter, J.; Vasantha, V. A.; Crombez, R.; Maniglia, R.; Slater, L.; Mourey, T., *Macromolecular Rapid Communications* **2012,** *33* (1), 69-74.

27. Shi, Z. X.; Newell, B. S.; Bailey, T. S.; Gin, D. L., *Polymer* **2014,** *55* (26), 6664-6671.

28. Agudelo, N. A.; Elsen, A. M.; He, H. K.; Lopez, B. L.; Matyjaszewski, K., *Journal of Polymer Science Part a-Polymer Chemistry* **2015,** *53* (2), 228-238.

29. Carrasco, P. M.; de Luzuriaga, A. R.; Constantinou, M.; Georgopanos, P.; Rangou, S.; Avgeropoulos, A.; Zafeiropoulos, N. E.; Grande, H. J.; Cabanero, G.; Mecerreyes, D.; Garcia, I., *Macromolecules* **2011,** *44* (12), 4936-4941.

30. Ahn, S.; Kwak, J.; Choi, C.; Seo, Y.; Kim, J. K.; Lee, B., *Macromolecules* **2017,** *50* (22), 9008-9014.

31. Lathrop, P. M.; Duan, Z. Y.; Ling, C.; Elabd, Y. A.; Kravaris, C., *Processes* **2019,** *7* (10).

32. Ye, Y. S.; Sharick, S.; Davis, E. M.; Winey, K. I.; Elabd, Y. A., *Acs Macro Letters* **2013,** *2* (7), 575-580.

33. Ye, Y. S.; Choi, J. H.; Winey, K. I.; Elabd, Y. A., *Macromolecules* **2012,** *45* (17), 7027-7035.

34. Moad, G.; Rizzardo, E.; Thang, S. H., *Australian Journal of Chemistry* **2005,** *58* (6), 379-410.

35. Moad, G.; Rizzardo, E.; Thang, S. H., *Australian Journal of Chemistry* **2006,** *59* (10), 669-692.

36. Moad, G.; Rizzardo, E.; Thang, S. H., *Accounts of Chemical Research* **2008,** *41* (9), 1133-1142.

37. Moad, G.; Rizzardo, E.; Thang, S. H., *Polymer* **2008,** *49* (5), 1079-1131.

38. Moad, G.; Rizzardo, E.; Thang, S. H., *Australian Journal of Chemistry* **2009,** *62* (11), 1402-1472.

39. Keddie, D. J.; Moad, G.; Rizzardo, E.; Thang, S. H., *Macromolecules* **2012,** *45* (13), 5321-5342.

40. Gardiner, J.; Martinez-Botella, I.; Tsanaktsidis, J.; Moad, G., *Polymer Chemistry* **2016,** *7* (2), 481-492.

41. Gardiner, J.; Martinez-Botella, I.; Kohl, T. M.; Krstina, J.; Moad, G.; Tyrell, J. H.; Coote, M. L.; Tsanaktsidis, J., *Polymer International* **2017,** *66* (11), 1438-1447.

42. Meek, K. M.; Elabd, Y. A., *Journal of Materials Chemistry A* **2015,** *3* (48), 24187-24194.

43. Ye, Y. S.; Elabd, Y. A., *Polymer* **2011,** *52* (5), 1309-1317.

44. Khandpur, A. K.; Forster, S.; Bates, F. S.; Hamley, I. W.; Ryan, A. J.; Bras, W.; Almdal, K.; Mortensen, K., *Macromolecules* **1995,** *28* (26), 8796-8806.

45. Bates, F. S.; Fredrickson, G. H., *Physics Today* **1999,** *52* (2), 32-38.

46. Matsen, M. W.; Schick, M., *Physical Review Letters* **1994,** *72* (16), 2660-2663.

47. Bailey, T. S.; Hardy, C. M.; Epps, T. H.; Bates, F. S., *Macromolecules* **2002,** *35* (18), 7007-7017.

48. Choi, J. H.; Ye, Y. S.; Elabd, Y. A.; Winey, K. I., *Macromolecules* **2013,** *46* (13), 5290-5300.

49. Shefelbine, T. A.; Vigild, M. E.; Matsen, M. W.; Hajduk, D. A.; Hillmyer, M. A.; Cussler, E. L.; Bates, F. S., *Journal of the American Chemical Society* **1999,** *121* (37), 8457-8465.

50. Epps, T. H.; Cochran, E. W.; Hardy, C. M.; Bailey, T. S.; Waletzko, R. S.; Bates, F. S., *Macromolecules* **2004,** *37* (19), 7085-7088.

51. Ludwigs, S.; Boker, A.; Abetz, V.; Muller, A. H. E.; Krausch, G., *Polymer* **2003,** *44* (22), 6815-6823.

52. Sato, T.; Ishida, Y.; Kameyama, A., *Polymer Journal* **2014,** *46* (4), 239-242.

53. Camps, M.; Chatzopoulos, M.; Camps, J. M.; Montheard, J. P., *Journal of Macromolecular Science-Reviews in Macromolecular Chemistry and Physics* **1987,** *C27* (3-4), 505-557.

54. Ting, W. H.; Dai, S. A.; Shih, Y. F.; Yang, I. K.; Su, W. C.; Jeng, R. J., *Polymer* **2008,** *49* (6), 1497-1505.

55. Zhu, M.; Zhang, X. J.; Wang, Y. G.; Wu, Y. B.; Wang, H.; Zhang, M.; Chen, Q.; Shen, Z. C.; Li, N. W., *Journal of Membrane Science* **2018,** *554*, 264-273.

56. Matsushima, S.; Takano, A.; Takahashi, Y.; Matsushita, Y., *Polymer* **2017,** *133*, 137-142.